Generalized UAV Selection With Distributed Transmission Policies

Petros S. Bithas, *Senior Member, IEEE*, and Aris L. Moustakas, *Senior Member, IEEE*

***Abstract*— Unmanned aerial vehicle (UAV)-aided communications is a promising emerging technology that will be adopted in the next generation communication networks. In this paper, a number of advanced cooperative UAV-aided communication solutions is proposed and evaluated, which considerably improve the performance of traditional terrestrial networks. Specifically, two generalized multi-UAV-selection schemes are introduced, depending on whether a direct link between the source and the destination is available or not. Once the UAVs have been selected, they may retransmit the source message to the destination using distributed space-time coding, or, in the presence of channel state information, distributed beamforming. A number of metrics to evaluate the performance on a realistic channel model was adopted, including the end-to-end outage probability (OP), the so-called goodput, and the average number of path estimations, as well as the total UAV communications power consumption. Exact expressions for the OP were obtained in terms of finite sums. Moreover, convenient closed-form expressions for the asymptotic OP were derived, valid for large numbers of UAVs, which are also very accurate for few UAVs. All results were compared with numerical simulations, which clearly depict the performance improvement induced by the proposed schemes as well as the impact of various system and channel parameters to the performance.**

***Index Terms*— Beamforming, distributed transmission policies, generalized relay selection, power consumption, space time coding, stochastic analysis, UAV-enabled communications.**

I. Introduction

UNMANNED aerial vehicles (UAVs) have recently drawn substantial attention of academic and industry communication technology research. The driving forces for constructing UAV-enabled communication networks include: i) their adaptability in extreme topographies, such as cliffs, valleys, and steep slopes, where access based on terrestrial networks is very difficult, ii) reduced CAPEX and OPEX in remote areas, iii) increased availability in disasters, like earthquakes, or in crowded events, and iv) enhanced probability for line-of-sight (LoS) conditions. Contrary to conventional ground networks, flying networks, accommodated with air-mounted transceivers, can be effectively deployed to reduce blocking, which is a major cause of signal attenuation in wireless links. Since terrestrial networks may often struggle in areas with obstacles, the highly mobile and dispersed UAV-nodes have a significant chance of achieving LoS (or near-LoS) links, as compared to the ground segments. Thus, they complement all types of ground networks in order to enhance coverage and connectivity [1]. In addition, swarms of UAVs can be employed to work cooperatively, in order to carry out complex tasks in significantly larger areas [2] and, especially, in monitoring and surveillance applications. The so-called flying ad-hoc networks (FANETs), in which multiple UAVs communicate in an ad-hoc manner, can effectively expand the connectivity in scenarios with terrestrial network constraints. In recent years, the use of UAVs as base stations, movable relays or autonomous communicating nodes has also attracted the interest of the research community, while 3GPP has suggested the employment of aerial vehicles for LTE communications [3]. Additionally, it is expected that future internet of things (IoT) deployments will include UAVs as autonomous communicating nodes for providing low latency and highly reliable connections in cities, across suburban areas, and in environments with no terrestrial wireless infrastructure [4].

Recently, the employment of UAVs in cooperative communication networks was proposed [5]. In this type of networks, UAVs can adjust their location to cope with the modifications of the communication environment, and UAV relay technology may be exploited to increase the system's communication range as well as its transmission quality. In this framework, different aspects of UAV-enabled cooperative networks have been studied in the past few years, e.g., secrecy performance analysis [6], optimal UAV placements [7], [8], energy harvesting scenarios [9], and intelligent reflecting surface UAV relaying [10]. Additionally, capitalizing on clusters of UAVs and in an effort to further improve network performance in a complexity-affordable manner, various UAV-selection strategies have been also proposed, e.g., [11], [12], [13], [14]. For example, in [11], two UAV selection strategies for multiple-UAV assisted relaying networks have been proposed, and their outage and coverage probabilities have been analytically investigated. In [12], a new UAV-selection policy is proposed, which exploits the stationarity of the shadowing and its performance was analytically evaluated and compared with empirical data. However, in these UAV selection strategies only one UAV-relay is employed in the second phase of communications.

Manuscript received 4 May 2022; revised 16 October 2022; accepted 6 December 2022. Date of publication 15 December 2022; date of current version 16 February 2023. This research was funded in part by the Office of Naval Research Global, with Grant No. N62909-18-1-2141 (2018-2021). The associate editor coordinating the review of this article and approving it for publication was F. Zhou. *(Corresponding author: Petros S. Bithas.)*

Petros S. Bithas is with the Department of Digital Industry Technologies, National and Kapodistrian University of Athens (NKUA), 34400 Psahna, Greece (e-mail: pbithas@dind.uoa.gr).

Aris L. Moustakas is with the Department of Physics, National and Kapodistrian University of Athens (NKUA), 15772 Athens, Greece (e-mail: arislm@phys.uoa.gr).

Color versions of one or more figures in this article are available at https://doi.org/10.1109/TCOMM.2022.3229665.

Digital Object Identifier 10.1109/TCOMM.2022.3229665

To include more UAV transmissions, a simple scheme that improves the performance (in terms of diversity order increase) of channel selection policies of wireless communication systems is the orthogonal space-time coding (STC) [15], [16]. For example, in [15] the symbol error rate performance of an STC system with a generalized minimum-selection combining receiver is presented and it is shown that the adoption of this scheme offers a reduction in complexity and processing power at the receiver. However, due to the signal processing and energy consumption constraints imposed by the limited UAV capabilities, as well as the reduced performance of STC (as a result of the antennas' spatial correlation), in practical scenarios, it is inefficient to consider multiple antennas mounted on the UAVs. Nevertheless, these limitations can be alleviated by adopting distributed STC (DSTC) protocols [17], and using several single-antenna cooperating UAVs. As a result, cooperative diversity can be exploited since UAVs are usually sufficiently separated, and thus have uncorrelated channels. This is why this approach has been followed in the past in studies related to cooperative (or not) communication networks, e.g., [18], [19], [20], [21], [22]. In [18], a new opportunistic DSTC relaying scheme is proposed, in which the set of relays that have successfully decoded the received signal from the source, jointly re-transmit it at the destination using the principles of DSTC. The main idea of this paper was extended in [19], in which the relay stations with the top received channel state information strength are selected to retransmit the packet using also DSTC approach. In both these studies, it was depicted that employing two relays in the second phase of communications offers an excellent compromise between performance improvement and complexity increase. Moreover, in [20], the cost and benefits of cooperative transmissions, based on STBC, for data broadcasting in vehicular networks has been investigated, revealing in various scenarios the advantages of cooperation. Furthermore, in [21], an experimental study for a DSTC-based cooperative relaying system was presented in two-hop relaying schemes. The results showed that DSTC-based cooperative relaying can improve the end-to-end (E2E) error performance in realistic environments. Therefore, recently, the area of distributed/collaborative communications has gained an increased interest as it is proved by the various contributions that have been reported.

The potential benefits of distributed beamforming have not been analyzed sufficiently. For example, in [23] and [24] a set of UAVs are used as a virtual antenna array, however without taking channel fading into account. Since experimental efforts have proved the potential of distributed beamforming in UAV-communications [25], it is important to further analyze its efficiency in more realistic scenarios.

As a result, despite the undoubtable advantages offered, the application of distributed STC/beamforming in UAV-enabled communication networks has not been thoroughly investigated. For example, in all the above studies, it has been concluded that an important challenge in distributed communication systems is to minimize extra control information exchanges for synchronization and coordination procedures. An approach towards that direction would be to exploit the valuable tool of DSTC only if it is necessary and only for a subset of the available UAVs. In this paper, motivated by the above, we analyze the potential benefits of selection-aided, distributed, UAV-enabled communication networks, using cooperation schemes, implemented by DSTC and distributed beamforming (DBF). More specifically, depending on the availability of the direct link, two UAV selection policies are proposed, which improve the overall network performance, while simultaneously take into account the signal processing/exchange/power constraints imposed by this type of communications. In summary, the main contributions of this paper can be categorized as follows:

- *Scenaria*: Two UAV-selection policies are proposed. In the first one, only communications through the (relay acting) UAVs is available. In the second one, a direct link between source and destination is also occasionally present, thus significantly reducing the total delay. In both scenaria, only a subset of UAVs is selected for relaying, based on the available channels state.
- *Cooperating Schemes:* The impact of DSTC and DBF UAV-aided cooperating communications schemes are analytically investigated in the presence of a realistic channel model, which takes into account various parameters of the UAV-enabled communications, including the impact of the pathloss, shadowing, and small-scale fading, as well as the presence or not of LoS components.
- *Performance Metrics:* Throughout the paper, the key metric used was the E2E outage probability (OP), taking into account both relay links to the UAVs. In addition, in order to obtain a more complete and detailed picture of the system's performance, various complementary performance metrics have been also adopted or proposed, for the first time in this type of communications. More specifically, for comparing the different delay behavior of the two scenarios, the goodput is calculated. The complexity of the UAV links is quantified using the average number of path estimations (ANPEs) required for the second relay link. Finally, the UAV communications power consumption at fixed OP is evaluated. Surprisingly, the communications power is not an increasing function of the number of UAVs, due to the presence of diversity, thus allowing us to optimize the total power consumption.
- *Analytic Tools*: Novel closed-form analytic solutions have been provided, in terms of simple and easy-to-evaluate functions. Moreover, we also included two asymptotic methods to further simplify the final expressions and to gain additional insight. Specifically, the high signal-to-noise ratio (SNR) behavior of the outage was calculated to showcase its tails, while based on saddle-point analysis, asymptotic expressions are obtained, valid in the limit of large UAV numbers, which provide compact and highly accurate estimate of the OP. More importantly, the latter one is easily generalizable to other channel models.

The rest of the paper is organized as follows. In Section II, the system and channel models are presented, while the performance metrics employed in this study are also provided. In Section III, the first scenario, which does not include a direct link between source and destination is analyzed, and its

TABLE I
PARAMETERS DEFINITION AND SIMULATION VALUES. THESE PARAMETER VALUES HAVE BEEN USED IN ALL FIGURES, EXCEPT THE ONES WHERE OTHER VALUES ARE EXPLICITLY SPECIFIED

Parameter	Definition	Value	Parameter	Definition	Value
λ	Wavelength	0.15cm	β_1	S curve parameter 1	12.8/9.61 (1st/2nd link)
P_t	S transmit power	8dBm	β_2	S curve parameter 2	0.11/0.16 (1st/2nd link)
P_r	UAVs transmit power	6dBm	ζ_{LoS}	LoS losses	1.6/1 (1st/2nd link)
L_s	Number of S antennas	1	ζ_{NLoS}	NLoS losses	23/20 (1st/2nd link)
L_d	Number of D antennas	1	d_D	Distance between UAVs-D	500m
M	Number of UAVs in 2nd leg	2	r_0	Radius of UAVs cluster	50m
K	Number of available UAVs	6	P_{cTx}	UAVs' Tx circuit powers	0.1W
N_0	Noise power	-97.8dBm	P_{cRx}	UAVs' Rx circuit powers	0.15W
m	Nakagami-m shaping	2	η	Drain efficiency	0.35
G_T	Transmit antenna gain	5dB	γ_R	Outage threshold	0dB
G_R	Receive antenna gain	5dB	$\alpha_{sr,rd,sd}$	Path loss factors	2.1/2.1/2.9
h	UAVs height	100m			

performance is investigated. In Section IV, the presence of a direct link is included and its impact analyzed. Finally, the conclusions are presented in Section V.

II. SYSTEM AND CHANNEL MODELS

In this section, the system and channel models under consideration are presented, the two operation scenarios are briefly described, and the performance metrics employed are introduced. In Table I, the definitions of most of the parameters involved in this study are included.

A. System Model

We consider a communications system, depicted in Fig. 1.a, between a source (S) and a destination (D) node at a distance d_D apart, equipped with L_s and L_d collocated antennas, respectively. The source intends to send a packet over a fixed time duration T encoded with rate R. To assist with the communication between S and D, a group of K single antenna UAVs located in the vicinity of S are used.[1] They are elevated at height h and are allowed to be mobile within a horizontal radius r_0 from the S location. Since r_0 is assumed to be small, LoS conditions are likely to be available between S and the UAVs. We assume that $r_0 \ll d_D$ and hence for simplicity all UAVs are taken at approximately the same distance d_D from D. Depending on the severity of the pathloss between S and D, we consider two distinct scenarios. In **Scenario 1**, no direct connectivity between S and D is available and hence communication between them is only possible through the UAVs acting as relays. Since the UAVs can operate at half duplex mode, communication proceeds in two phases. In the first, S transmits the packet over $T/2$ channel uses to the UAVs (**Leg 1**). The transmission mode over the L_s antennas is assumed to take place using STC. If N is the (random) number of UAVs that successfully decoded the message, then over the second phase of communication, lasting $T/2$ channel uses, a subset of $\min(M, N)$ UAVs retransmit the message with the same rate R to D, where M is a predefined number of UAVs that should be involved in the second communication phase, with the stronger SNRs (**Leg 2**). This approach results to various practical advantages, including signaling reduction, signal processing simplification, which are very important for UAV-enabled communications that are characterized by well-known energy consumption constraints. Depending on the available knowledge, by each UAV of its channel to D, DBF among the UAVs in (**Leg 2**) may be employed.

In **Scenario 2**, the possibility of successfully decoding the message at D over the first phase of communications is also considered (**Leg 0**), thus significantly increasing the average rate. When this is the case, of course, due to their proximity to the S, it is reasonable to assume that all UAVs successfully decode the message over the first phase. In this scenario, when the received message at D over the first phase does not justify an SNR-based criterion, the UAVs that have successfully decoded the signal proceed in the second phase by re-transmitting the message. Then, the D can combine the signals received over both transmission phases. To help keep the UAV-power consumption low, we also analyze a scheme of not employing the UAVs unless the SNR of the direct link is quite low. Moreover, in Fig. 1.b, the framework structure of the proposed scheme is also presented. In this figure, the two legs of communication are depicted, as well as the main parts of procedure followed by all network elements in order to realize the communication. Motivating scenarios that the system model assumed can be applied include surveillance operations (or disaster managements scenarios) [26] and in UAV-aided urban macro-cell networks with users located far away from the BS [27].

B. Channel Model

In this paper, all links are assumed to undergo block fading, thereby having constant channel coefficients within each block of data.[2] Moreover, these coefficients change independently from one block to the other. In this context, the generalized Nakagami-m fading model has been considered, which has been found to accurately model UAV-to-ground small scale fading conditions [28], since it captures the intermediate situation of having both LoS and fading components. This

[1]It is noted that the K UAVs that can be used for communication purposes have adequate battery supplies during both communication phases described later on.

[2]This constancy assumption is approximately correct and hence inbetween pilot measurements, channels are perfectly tracked.

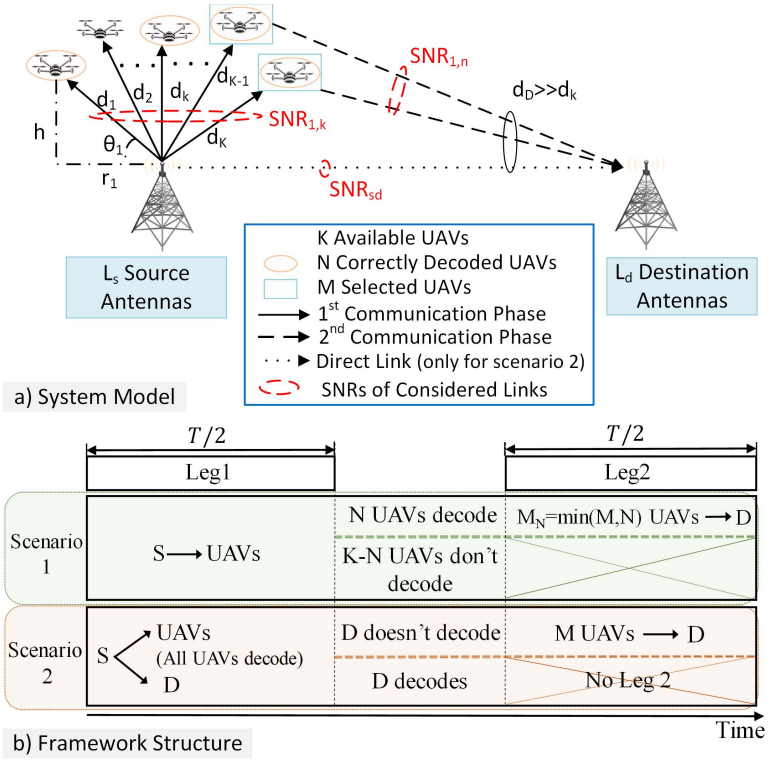

Fig. 1. System model and framework structure.

particular fading distribution can be used in communication scenarios, in which LoS conditions occur in high probability, e.g., in sub-urban or rural environments In fact, it has been claimed that a one-to-one mapping between the Nakagami-m shaping parameter and the Ricean K factor, allowing the Nakagami distribution to accurately approximate the corresponding Ricean one [29].

In this context, the probability density function (PDF) of the channel gain due to the multipath fading, is given by [29, eq. (2.20)]

$$f(x) = \frac{m^m x^{m-1}}{\Omega^m \Gamma(m)} \exp\left(-\frac{mx}{\Omega}\right), \tag{1}$$

where m is distribution's shaping parameter, related to the severity of the fading, i.e., as m increases LoS conditions are approximated, Ω denotes the mean square value, and $\Gamma(\cdot)$ is the gamma function [30, eq. (8.310/1)]. As far as the shadowing behavior is concerned, a deterministic modeling approach for the large scale fading is followed that was proposed in [31]. According to this, the expectation of the excessive pathloss has been studied, as it will be shown in more details in Section III.A.

C. Performance Metrics

Before analyzing the communications system for each scenario separately, we briefly introduce the performance metrics that we will use to assess the performance of each solution.

1) End-to-End Outage Probability: The OP is defined as the probability that the transmitted packet with a given R does not get decoded during transmission. Hence, the OP depends on whether the packet got successfully decoded over the first and/or second communications phase.

2) Goodput: A quantity dual to the OP is the so-called communications goodput, which corresponds to the ratio of the number of bits successfully transmitted over the allotted communications duration. This quantity is essentially the transmitted rate times the success-probability of transmission at this rate and is useful to compare transmissions with different communications duration, such as in Scenarios 1 and 2.

3) Signalling Overhead: The signalling overhead of the proposed schemes will be evaluated using the ANPEs as a complexity criterion. In particular, as the number of path estimations at the 2^{nd} link increases, higher amount of signalling must be exchanged in order to support the communication procedure. It is noted that the ANPE is directly related to the type and number of comparisons that are required to be performed [32].

4) UAVs Communication Power Consumption: Since power consumption is a critical factor for UAVs efficient functioning, a power consumption analysis is also presented. In particular, the number of UAVs and the resulting power consumed are investigated for achieving an OP target at the 2^{nd} communication phase. To this aim, we will model power consumption following the approach presented in [33] and [34]. Moreover, it is assumed that all circuits work in the active mode, since there is always a signal to be transmitted/received. Both these assumptions will not alter the main findings of the analysis. In this context, the total power consumption, P_{tot}, of all UAVs can be expressed as

$$P_{\text{tot}} = P_{cRx} \cdot K + M \cdot \left((\omega + 1) P_r + P_{cTx}\right), \tag{2}$$

where P_{cTx}, P_{cRx} denote the UAVs' transmitter and receiver circuit powers, respectively. Moreover, in (2), ω denotes the amplifier power efficiency given by $\omega = \frac{2\sqrt{2^R}-1}{\eta\sqrt{2^R}+1} - 1$, with η denoting the drain efficiency, R the transmission rate, while P_r denotes the UAVs' transmit power. Hence, the power consumption optimization problem can be formulated as

$$\begin{aligned} \min_{K} \quad & P_{\text{tot}}(P_r, K) \\ \text{subject to} \quad & P_{\text{out}}(P_r, K) = p^*, P_r > 0, K > 0, \end{aligned}$$

where p^* denotes the OP target. For concreteness, we have specified the dependence of P_{out} on P_r and K. The last OP expression is inverted to express P_r as a function of K for fixed outage.

III. Scenario 1: Two-Hop Communications

In this section, the first scenario will be discussed, in which there is no availability of a direct link between S and D.

A. Leg 1: Communication From Source to UAV Cluster

In this leg of communication, the signal is transmitted with the aid of L_s antennas by the S to each of the K single-antenna UAVs, employing STC between the L_s transmit antennas for maximum diversity gain. Thus, the received SNR of the kth UAV can be expressed as

$$\text{SNR}_{1,k} = \overline{\gamma}_{1k} \sum_{\ell=1}^{L_s} x_{\ell k}, \tag{3}$$

where $x_{\ell k}$ is the normalized modulus squared of the channel coefficient between source antenna ℓ and UAV k. The quantities $x_{\ell k}$ are assumed independent and identically distributed (i.i.d.) random variables (RVs) following the Nakagami-m distribution described by (1). The mean SNR coefficient $\overline{\gamma}_{1k}$ for UAV k, takes into account the probability of LoS for UAV-enabled communications and is given by [14]

$$\overline{\gamma}_{1k} = \frac{P_t}{N_0} \left(\frac{G_T G_R \lambda^2}{16\pi^2 d_k^{a_{sr}}} \right) 10^{-\frac{PL_{\text{dB,k}}}{10}}, \tag{4}$$

where G_T, G_R denote the transmitter/receiver antenna gains, respectively, P_t the S transmit power, λ the wavelength, and the additional path loss due to the LoS probability given by

$$PL_{\text{dB,k}} = P_{\text{LoS,k}} \zeta_{\text{LoS}} + P_{\text{NLoS,k}} \zeta_{\text{NLoS}}, \tag{5}$$

with

$$P_{\text{LoS}} = \frac{1}{1 + \beta_1 \exp(-\beta_2(\theta_k - \beta_1))}.$$

Furthermore, $\theta_k = \tan^{-1} \frac{h}{r_k}$, the height h is assumed to be equal for all UAVs, while r_k denotes the ground distance between the S and UAV k, $d_k = \sqrt{h^2 + r_k^2}$, and a_{sr} is the path loss exponent. Moreover, $P_{\text{NLoS,k}} = 1 - P_{\text{LoS,k}}$, is the probability of non-LoS or *shadow-blocked* transmission, while coefficients β_1, β_2 and $\zeta_{\text{LoS}}, \zeta_{\text{NLoS}}$ (related to the losses of the LoS and shadowed connections, respectively), have been empirically evaluated for various scenarios in [31] and [35]. Based on the system model assumed, in (3), where $\text{SNR}_{1,k}$ is defined, the sum of identical distributed gamma RVs is presented, with cumulative distribution function (CDF) $F_{1k}(x)$, been obtained in [36]

$$F_{1k}(x) = \gamma \left(mL_s, \frac{m}{\overline{\gamma}_{1k}} x \right), \tag{6}$$

where $\gamma(a, x) = \int_0^x t^{a-1} e^{-t} dt / \Gamma(a)$ denotes the normalized lower incomplete gamma function [30]. $F_{1k}(x)$ corresponds to the OP of UAV k, with instantaneous received SNR x. We see that $F_{1k}(x)$ depends on the UAV through its horizontal position r_k. However, since in practical scenarios, UAVs are characterized by random mobility, this distance is time-varying, and thus a more relevant metric for the OP of each UAV is its average with respect to r_k over a disk of radius r_0, given by

$$F_1(x) = \frac{2}{r_0^2} \int_0^{r_0} r_k \, dr_k \gamma \left(mL_s, \frac{mx}{\bar{\gamma}_{1k}} \right). \tag{7}$$

For transmission rate R, the average OP is $F_1(\gamma_{\text{R}})$, with instantaneous SNR threshold given by

$$\gamma_{\text{R}} = 2^R - 1. \tag{8}$$

For the next transmission leg, we will need the distribution of the number UAVs that have successfully decoded the message. Given that each UAV may decode independently from all others, the probability that N UAVs decode the message will simply be binomial, i.e.,

$$\Pi_N(\gamma_{\text{R}}) = \binom{K}{N} F_1(\gamma_{\text{R}})^{K-N} (1 - F_1(\gamma_{\text{R}}))^N. \tag{9}$$

where $F_1(\cdot)$ is given in (7).

B. Leg 2: Communication From Selected UAVs to Destination

In this phase of communications, the UAVs that successfully decoded the message in Leg 1 cooperate to retransmit the message in a distributed fashion to D. We assume symbol-level synchronization and perfect channel knowledge at D, which can then coordinate the transmission, similar to [17] and [18]. Depending on whether channel information is available at UAVs or not, we will discuss two different modes of operation.

1) Open Loop: No Channel Information at UAVs: The UAVs that have successfully decoded the message can participate in the second communication phase. For a given UAV with index $n \in [1, N]$, where N is the random number of available UAVs, the received SNR at D takes the form

$$\text{SNR}_{2,n} = \overline{\gamma}_2 \sum_{\ell=1}^{L_d} y_{n\ell}, \tag{10}$$

where $y_{n\ell}$ is the normalized modulus squared of the channel coefficient between UAV n and D antenna ℓ. We assume that $y_{n\ell}$ are i.i.d. RVs and follow the Nakagami-m distribution. Moreover, $\overline{\gamma}_2$ is the mean SNR from each UAV to D, which takes the form

$$\overline{\gamma}_2 = \frac{P_r}{N_0} \left(\frac{G_T G_R \lambda^2}{16\pi^2 d_D^{a_{rd}}} \right) 10^{-\frac{PL_{\text{dB}}}{10}}, \tag{11}$$

where P_r is assumed to be equal for all UAVs, and the distance d_D is also assumed equal for all UAVs. As Leg 1, the CDF of

$\text{SNR}_{2,n}$ is $\mathbb{P}(\text{SNR}_{2,n} < \overline{\gamma}_2 x/m) = \bar{F}_2(x)$, where $\mathbb{P}(\cdot)$ denotes probability and $\bar{F}_2(x)$ can be expressed as [36]

$$\bar{F}_2(x) = \gamma\left(mL_d, x\right). \tag{12}$$

For a given instantiation of the UAV $\text{SNR}_{2,n}$'s, we order the SNRs at D in a descending order of indices.[3] From the N UAVs, the $M_N = \min(M, N)$ with the highest SNR at D will participate in the next communication phase, where parameter M can be chosen to maximize a performance criterion. In the absence of channel information at the UAVs, the M_N UAVs will cooperatively transmit the message using DSTC. Each transmitting UAV is assigned a column from the space-time code matrix [38]. This scheme, where the number of transmitters is unknown and random, can be implemented in an uncoordinated manner, using an approach presented in [39] or assuming some form of centralized control, e.g., [20]. For the selected subset of UAVs, and due to the orthogonality property, the instantaneous received SNR at D, can be expressed as [18]

$$\text{SNR}_{2,\text{st}} = \sum_{n=1}^{M_N} \text{SNR}_{2,n} = \overline{\gamma}_2 \sum_{n=1}^{M_N} \sum_{\ell=1}^{L_d} y_{n\ell}. \tag{13}$$

Based on [40], it is not difficult to recognize that the CDF of $\text{SNR}_{2,\text{st}}$ can be expressed as

$$F_{2,\text{st}}^{M,N}(x) = M\binom{N}{M} \int_0^\infty dx_M \bar{f}_2(x_M) \bar{F}_2(x_M)^{N-M} \cdot \prod_{i=1}^{M-1} \int_{x_M}^\infty dx_i \bar{f}_2(x_i) \Theta\left(mx - \overline{\gamma}_2 \sum_{i=1}^{M} x_i\right), \tag{14}$$

where $\bar{f}_2(x) = \bar{F}_2'(x)$ and $\Theta(x)$ is the unit step function, with unit value for $x > 0$ and zero otherwise. The combinatorial factor corresponds to the number of ways $M-1$ i.i.d. RVs being greater than x_M, while $N-M$ being less than x_M. It is straightforward to show that the above integral for $M = N$ becomes

$$F_{2,\text{st}}^{M,M}(x) \ = \gamma\left(mL_d M, \frac{mx}{\overline{\gamma}_2}\right). \tag{15}$$

For $M < N$, its expression is more complicated and can be summarized in the following proposition.

Proposition 3.1: (Exact Outage $F_{2,\text{st}}^{M,N}(x)$ for DSTC: $M < N$): Let m be a positive integer and $M < N$. Then the multiple integral in (14) *can be expressed in the following exact form*

$$F_{2,\text{st}}^{M,N}(x) = \mathcal{C}_1 \gamma\left(mL_d M, \frac{mx}{\overline{\gamma}_2}\right) + \sum_{\substack{i_1 \sim M \\ n_i}} \mathcal{B}\left[\mathcal{C}_2 \gamma\left(k+1, \frac{m(M+i_M)x}{M\overline{\gamma}_2}\right) + \mathcal{C}_3 \gamma\left(k+1, \frac{mx}{\overline{\gamma}_2}\right)\right], \tag{16}$$

[3]Such an approach can be performed in either a centralized manner, by using a central controller in the network, or in a distributed manner, by employing the methodology of distributed timers [37].

where

$$\mathcal{C}_1 = \frac{N!}{M!} \sum_{i_1 \sim M} \left[\prod_{j=1}^{M-1} \frac{\Gamma(mL_d + i_j)}{i_j! \Gamma(mL_d)}\right] \frac{\prod_{j=2}^{M-1} j^{i_j - mL_d - i_{j-1}}}{M^{mL_d + i_{M-1}}},$$

$$\mathcal{C}_2 = \sum_{k=0}^{p_1-1} \frac{(-p_1+1)_k}{(2-p_M)_k} \left(\frac{i_M}{M}\right)^k \left(\frac{i_M + M}{M}\right)^{k+1},$$

$$\mathcal{C}_3 = \sum_{k=0}^{q_1-1} \frac{(1-q_1)_k}{(2-p_M)_k} \left(-\frac{i_M}{M}\right)^k,$$

with $(a)_k = \Gamma(a+k)/\Gamma(a)$ denoting the Pochhammer symbol, while $p_n = nmL_d + S_M$, $q_n = (M-n)mL_d + yi_{M-1}$ and $S_M = 0n_1 + 1n_2 \cdots (M-1)n_M$.

Proof: The proof for the derivation of (16) and the definition of $\mathcal{B}$ can be found in Appendix A. It should be stressed that the above results involve multiple finite sums, which always converge and can be evaluated in a simple numerical fashion. ■

Corollary 3.1 (High SNR Outage $F_{2,\text{st}}^{M,N}(x)$ for DSTC): In the limit $\frac{x}{\overline{\gamma}_2} \ll 1$, the CDF of $\text{SNR}_{2,\text{st}}$ becomes asymptotically equal to

$$F_{2,\text{st}}^{M,N}(x) \approx \mathcal{H}\left(\frac{mx}{\overline{\gamma}_2}\right)^{mL_d N}, \tag{17}$$

where

$$\mathcal{H} = \frac{M\binom{N}{M}}{\Gamma(mL_d N + 1)} \frac{\Gamma(mL_d + 1)^{M-N}}{\Gamma(mL_d)} \cdot \prod_{j=1}^{M-1} \sum_{k_j=0}^{mL_d - 1} \frac{1}{k_j!} \frac{\Gamma(\sum_j k_j + mL_d(N+1-M))}{M^{\sum_j k_j + mL_d(N+1-M)}}. \tag{18}$$

Proof: See Appendix B. ■

The above result suggests that the large SNR is asymptotically governed by the event where all N UAVs participating in Leg 2 have very small x, independent of how many M are used.

While the expression for the CDF in the above proposition is exact, it is not always easy to be manipulated. Therefore, we provide an easy-to-evaluate closed-form expression for $F_{2,\text{st}}^{M,N}(x)$, which is valid in the asymptotic limit $N, M \to \infty$ with fixed ratio $\beta = \frac{M}{N} < 1$

Proposition 3.2: (Asymptotic Outage $F_{2,\text{st}}^{M,N}(x)$ for DSTC: $M < N$): Assume $\beta < 1$ and define

$$\overline{Q}_{2,\text{st}}^{M,N}(z) = \frac{\sqrt{\beta}}{y_0 \sqrt{(1-\beta)|\phi_{yy}|}} e^{N\left[\phi(y_0, s_0; z) + \frac{1}{2} s_0^2 \left(\phi_{ss} - \frac{\phi_{ys}^2}{\phi_{yy}}\right)\right]} \cdot Q\left(\sqrt{N s_0^2 \left(\phi_{ss} - \frac{\phi_{ys}^2}{\phi_{yy}}\right)}\right). \tag{19}$$

Then let

$$\overline{P}_{2,\text{st}}^{M,N}(z) = \begin{cases} \overline{Q}_{2,\text{st}}^{M,N}(z) & \text{if } z < z_{erg} \\ 1 - \overline{Q}_{2,\text{st}}^{M,N}(z) & \text{if } z > z_{erg}, \end{cases} \tag{20}$$

where a)

1) $\phi(y,s;z)$ *is given by*

$$\phi(y,s;z) = \beta z s + (1-\beta)\log\left[\frac{\gamma\left(mL_d, \frac{t(y)}{1+s}\right)}{1-\beta}\right] + \beta\log\left(\frac{y}{\beta}\right) - \beta m L_d \log(1+s), \quad (21)$$

2) $t(y)$ *is the solution of* $1-y=\gamma(mL_d,t)$
3) y_0, s_0 *are the solutions of the fixed point equations*

$$\frac{\partial\phi}{\partial y} = \frac{\partial\phi}{\partial s} = 0, \quad (22)$$

4) $Q(y)=\int_y^\infty \frac{dx}{\sqrt{2\pi}} e^{-\frac{x^2}{2}}$ *is the usual Q-function,*
5) $\phi_{yy}, \phi_{ys}, \phi_{ss}$ *are the second partial derivatives of* ϕ *with respect to the indices (i.e.,* $\phi_{yy} = \frac{\partial^2\phi}{\partial y^2}$*), evaluated at* y_0, s_0*, and*
6) z_{erg} *is the solution of* (22) *for* $s=0$ *and corresponds to the most probable value of the asymptotic distribution.*

Then, for every $z>0$ *the CDF of the normalized value of* $SNR_{2,\mathrm{st}}$ *converges to* $\overline{P}_{2,\mathrm{st}}^{M,N}(z)$ *in the sense*

$$\lim_{N\to\infty} N\left|F_{2,\mathrm{st}}^{M,N}\left(\frac{\overline{\gamma}_2 M z}{m}\right) - \overline{P}_{2,\mathrm{st}}^{M,N}(z)\right| < \infty. \quad (23)$$

Proof: The proof of the above is based on saddle-point analysis given in [41] and can be found in Appendix C. Further details on the proof can be found in [42]. ■

From the above Proposition we conclude that $F_{2,\mathrm{st}}^{M,N}(x) \approx \overline{P}_{2,\mathrm{st}}^{M,N}\left(\frac{mx}{M\overline{\gamma}_2}\right)$.

Remark 1: While the details of the proof and the solution appear in the Appendix, it is worth providing some details here on the basic steps taken to evaluate the asymptotic result. Initially, one needs to evaluate the saddle-point values of y_0, s_0*, by finding the roots of the saddle point equations, which appear in compact form in* (22)*. Once these are evaluated, then the evaluation of the outage probability is a straightforward evaluation of the function* ϕ *in equation (21) and its second partial derivatives with respect to the first two arguments, namely* $\phi_{yy}, \phi_{ys}, \phi_{ss}$*, and then plugging these values in* (19)*. A similar procedure should take place in other propositions below.*

To assess the validity of the exact expressions in Prop. 3.1 and the accuracy of the asymptotic results in Prop. 3.2, in Fig. 2a, the PDF and the CDF of $\mathrm{SNR}_{2,\mathrm{st}}$ obtained as above are compared with numerically simulated curves. The excellent agreement of the analytic expressions and the tightness of the asymptotic results, even for small numbers of UAVs, can be clearly seen. It should be stressed that this asymptotic method can be applied to all systems for which the CDF $\bar{F}_2(x)$ of each channel from the UAV to the receiver has an analytic expression.

2) Distributed Beamforming: Perfect Channel Information at UAVs: In this subsection, we will explore the outage performance of the 2^{nd} Leg when channel information is available at the individual UAVs. For simplicity, we will operate with a single antenna at D, i.e., $L_d = 1$. This

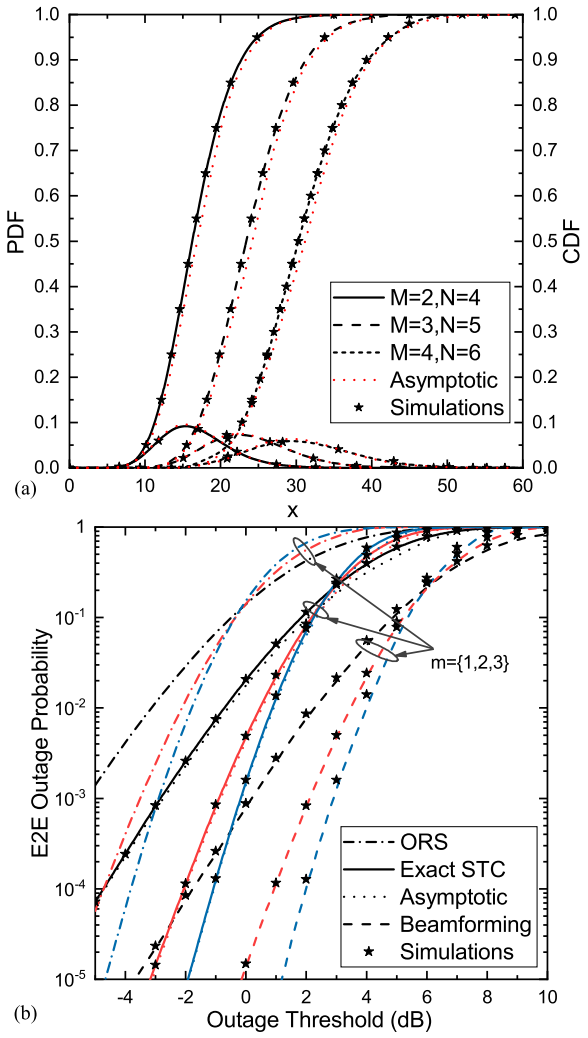

Fig. 2. (a) Plots of the PDF and the CDF from Prop. 3.1 (exact) and Prop. 3.2 (asymptotic) vs $x=\gamma_R/\bar{\gamma}_2$ for various numbers of N, M, with $L_d=2$, $m=2$, and $\bar{\gamma}_2=5$dB. Excellent agreement between exact and asymptotic is observed. (b) E2E OP vs. γ_R for different values of m (based on the parameters shown in Table I). Performance improves as m increases.

information can be obtained through closed loop or open loop synchronization [43], [44], [45]. In such a case, the optimal strategy for each UAV, operating on its own maximum power constraint, is to multiply its signal with the inverse phase of its channel to D. Hence, if the normalized channel of UAV n to D is $h_n = \sqrt{y_n}e^{i\phi_n}$, then the optimal weight will be $w_n = e^{-i\phi_n}$. As a result, if we choose the $M_N = \min(M,N)$ UAVs with the strongest SNR to D, the total SNR will be

$$\mathrm{SNR}_{2,\mathrm{bf}} = \overline{\gamma}_2\left(\sum_{n=1}^{M_N}\sqrt{y_n}\right)^2. \quad (24)$$

For general $M<N$, a closed-form expression of the CDF of $\mathrm{SNR}_{2,\mathrm{bf}}$, $F_{2,\mathrm{bf}}^{M,N}(x)$, does not exist. However, an asymptotic expression for $M,N\to\infty$ can be evaluated following the same approach as in Proposition 3.2.

Proposition 3.3: (Asymptotic Outage $F_{2,\mathrm{bf}}^{M,N}(x)$ *for BF:* $M<N$*): Let*

$$\overline{Q}_{2,\mathrm{bf}}^{M,N}(z) = \frac{\tilde{F}_t(t_0,s_0)\sqrt{\beta}}{\tilde{F}(t_0,s_0)\sqrt{(1-\beta)|m_{tt}|}}$$

$$\cdot e^{N\left[\phi(t_0,s_0;z)+\frac{1}{2}s_0^2\left(\phi_{ss}-\frac{\phi_{ts}^2}{\phi_{tt}}\right)\right]} Q\left(\sqrt{Ns_0^2\left(\phi_{ss}-\frac{\phi_{ts}^2}{\phi_{tt}}\right)}\right). \quad (25)$$

Then let

$$\overline{P}_{2,\mathrm{bf}}^{M,N}(z)=\begin{cases}\overline{Q}_{2,\mathrm{bf}}^{M,N}(z) & \text{if } z<z_{erg}\\ 1-\overline{Q}_{2,\mathrm{bf}}^{M,N}(z) & \text{if } z>z_{erg},\end{cases} \quad (26)$$

where

1) $\phi(t,s;z)$ *is given by*

$$\phi(t,s;z)=s\beta\sqrt{z}+\beta\log\left[\frac{\tilde{F}(t,s)}{\beta}\right]+(1-\beta)\log\left(\frac{\gamma(mL_d,t)}{1-\beta}\right) \quad (27)$$

2) $\tilde{F}(t,s)$ *is given by*

$$\tilde{F}(t,s)=\int_t^\infty dx\frac{x^{m-1}e^{-x-s\sqrt{x}}}{\Gamma(m)}=\frac{(-1)^{2m-1}2\sqrt{\pi}}{\Gamma(m)}\frac{\partial^{2m-1}}{\partial s^{2m-1}}\left[e^{\frac{s^2}{4}}Q\left(\frac{s+2\sqrt{t}}{\sqrt{2}}\right)\right] \quad (28)$$

and $\tilde{F}_t(t,s)$ *is its first partial derivative with respect to* t.

3) y_0, s_0 *are the solutions of the fixed point equations*

$$\frac{\partial\phi}{\partial y}=\frac{\partial\phi}{\partial s}=0 \quad (29)$$

4) $\phi_{tt},\phi_{ts},\phi_{ss}$ *are the second partial derivatives of* ϕ *with respect to the indices (i.e.,* $\phi_{tt}=\frac{\partial^2\phi}{\partial t^2}$*, etc.), evaluated at* t_0,s_0*, and*

5) z_{erg} *is the solution of* (29) *for* $s=0$ *and corresponds to the most probable value of the asymptotic distribution.*

Then, for every $z>0$ *the CDF of the normalized value of* $\sqrt{SNR_{2,\mathrm{bf}}}$, $F_{2,\mathrm{bf}}^{M,N}(x)$ *converges to* $\overline{P}_{2,\mathrm{bf}}^{M,N}(z)$ *in the sense*

$$\lim_{N\to\infty} N\left|F_{2,\mathrm{bf}}^{M,N}\left(\frac{\overline{\gamma}_2M^2z}{m}\right)-\overline{P}_{2,\mathrm{bf}}^{M,N}(z)\right|<\infty. \quad (30)$$

Proof: We first note that

$$\sqrt{\mathrm{SNR}_{2,\mathrm{bf}}}=\sqrt{\overline{\gamma}_2}\sum_{m=1}^{M}\sqrt{y_n}, \quad (31)$$

which means that $\sqrt{\mathrm{SNR}_{2,\mathrm{bf}}}$ can be expressed as a sum of independent variables. We therefore define the RV $\sqrt{Z}=\frac{1}{M}\sqrt{\frac{m\mathrm{SNR}_{2,\mathrm{bf}}}{\overline{\gamma}_2}}$ and proceed along the same lines as in Proposition 3.2. ■

The case $M=N$ is somewhat simpler, but still the distribution of $\mathrm{SNR}_{2,\mathrm{bf}}$ for general M is non-trivial [46]. However, we can obtain an analytic expression valid for large M as follows:

Proposition 3.4: (Asymptotic Outage $F_{2,\mathrm{bf}}^{M,N}(x)$ *for BF:* $M=N$*): Let*

$$\overline{Q}_{2,\mathrm{bf}}^{M,M}(z)=e^{M\left[\phi(s_0;z)+\frac{1}{2}s_0^2\phi_{ss}\right]}Q\left(\sqrt{Ms_0^2\phi_{ss}}\right). \quad (32)$$

Then let

$$\overline{P}_{2,\mathrm{bf}}^{M,M}(z)=\begin{cases}\overline{Q}_{2,\mathrm{bf}}^{M,M}(z) & \text{if } z<z_{erg}\\ 1-\overline{Q}_{2,\mathrm{bf}}^{M,M}(z) & \text{if } z>z_{erg},\end{cases} \quad (33)$$

for $z_{erg}=\frac{\Gamma(m+\frac{1}{2})}{\Gamma(m)}$ *and where*

1) $\phi(s;z)$ *is given by*

$$\phi(t,s;z)=s\sqrt{z}+\log\left[\frac{\tilde{F}(0,s)}{\beta}\right] \quad (34)$$

2) s_0 *is the solution of the fixed point equation*

$$\frac{\partial\phi}{\partial s}=0=z+\frac{\partial\log\tilde{F}(0,s)}{\partial s} \quad (35)$$

3) ϕ_{ss} *is the second partial derivatives of* ϕ *with respect to* s*, evaluated at* s_0.

Then for every $z>0$ *the CDF of the normalized value of* $\sqrt{SNR_{2,\mathrm{bf}}}$, $F_{2,\mathrm{bf}}^{M,M}(x)$ *converges to* $\overline{P}_{2,\mathrm{bf}}^{M,M}(z)$ *in the sense*

$$\lim_{M\to\infty} M\left|F_{2,\mathrm{bf}}^{M,M}\left(\frac{\overline{\gamma}_2M^2z}{m}\right)-\overline{P}_{2,\mathrm{bf}}^{M,M}(z)\right|<\infty. \quad (36)$$

Proof: To prove this, we start from the observation that now the moment-generating function (MGF) of z takes the simpler form

$$\overline{M}_{2,\mathrm{st}}^{M,M}(s)=\tilde{F}(0,s)^M, \quad (37)$$

where $\tilde{F}(0,s)$ is defined in (28). From here, we use the same tools discussed in Appendix C to obtain the final result. ■

Based on the above two propositions, $F_{2,\mathrm{bf}}^{M,N}(x)\approx\overline{P}_{2,\mathrm{bf}}^{M,N}\left(\frac{mx}{\overline{\gamma}_2M^2}\right)$.

C. Performance Analysis of Scenario 1

We will now use the above results to quantify the performance of the full link.

1) End-to-End Outage Probability: To obtain the E2E OP, we combine the probability of a fixed number N of UAVs to have decoded the packet on the first leg of communication, (7), with the OP of the second leg as follows:

$$P_{\mathrm{out}}=\sum_{N=0}^{K}\Pi_N(\gamma_R)F_{2,x}^{M_N,N}(\gamma_R)=\sum_{N=0}^{K}\binom{K}{N}F_1(\gamma_{\mathrm{R}})^{K-N}(1-F_1(\gamma_{\mathrm{R}}))^NF_{2,x}^{M_N,N}(\gamma_R), \quad (38)$$

where $M_N=\min(M,N)$, γ_R is given in (8) and $F_1(x)$ is the OP between S and each UAV given in (7). The term $F_{2,x}^{M_N,N}(\gamma_R)$ denotes the OP between N UAVs and D, where we can use either $F_{2,\mathrm{st}}^{M_N,N}(\gamma_R)$ (evaluated in Prop. 3.1 or asymptotically in Prop. 3.2) for DSTC, or $F_{2,\mathrm{bf}}^{M_N,N}(\gamma_R)$ (evaluated in Props. 3.3-3.4 for DBF). Note that for $M\geq N$, since $M_N=N$ the OP in the second leg used is taken from (15) and (33). In Table I, if not otherwise stated, the parameters considered at the simulation results are presented, which are based on previous studies, e.g., [47]. It is noted that the exact and high SNR analytical expressions for the E2E OP have

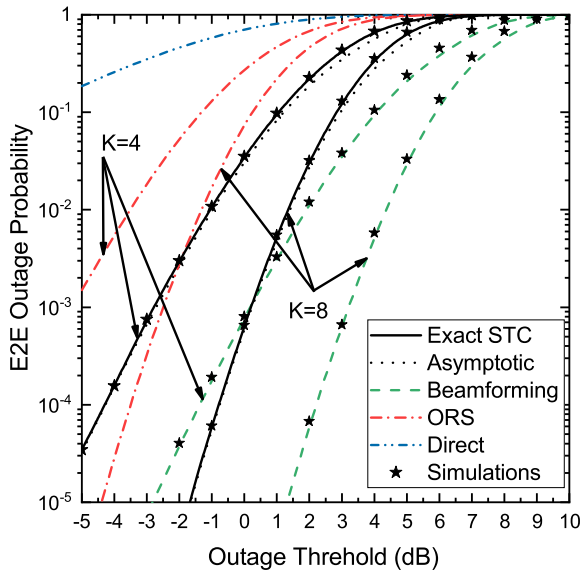

(a)

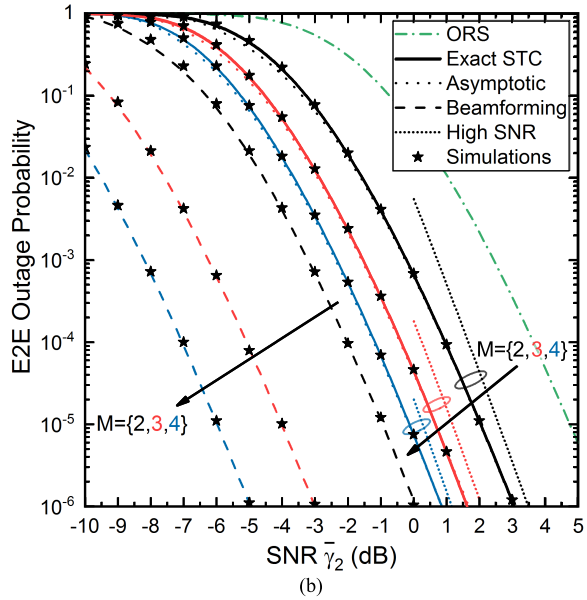

(b)

Fig. 3. (a) E2E OP vs. γ_R for $K = 4, 8$ in the absence of a direct link (based on the parameters shown in Table I). DBF provides the best performance. (b) E2E OP vs. $\bar{\gamma}_2$ for different maximum number of UAVs M employed in Leg 2 for Scenario 1. High SNR asymptotic results are quite close to the exact ones.

been numerically evaluated using the Mathematica™ software package, while the ones derived for high values of M, N have been evaluated using Matlab™ software package.

To understand the dependence of the E2E OP on various parameters, we will present a number of figures. In Fig. 2b, the E2E OP of Scenario 1 has been plotted as a function of γ_R for both DSTC and DBF modes of communications and for different channel fading models and Nakagami-m shaping parameters.[4] It is shown that in all scenarios the performance improves as m increases. However, this improvement is reduced for higher values of m. It is noteworthy that as m increases, the rate of the performance improvement is quite similar for all scenarios under investigation. Finally, it is also shown the tight approximation that is obtained by the asymptotic results. In Fig. 3a, we plot the E2E OP of Scenario 1 for both DSTC and DBF modes of communications for different values of the available UAVs K. For comparison purposes, we also plot the curves for 2 benchmarks, namely a scenario without UAV-aided communications (named direct) and a scenario in which opportunistic UAV-relay selection (ORS) is performed. In all cases, the schemes presented in this paper clearly improve the performance of the system. In addition, we observe that DBF has superior performance to DSTC, providing roughly a 3dB gain compared to it. In the same figure, the asymptotic curves for DSTC and DBF, obtained from Prop. 3.2 and Prop. 3.3, respectively, are also included, depicting an excellent agreement with exact results and simulations, even for the relatively small number of UAVs that is assumed.

To understand the behavior of the OP as a function of the received SNR, rather than the input rate R, which is parameterized with γ_R, in Fig. 3b, the E2E OP of Scenario 1 is plotted as a function of the average received SNR at D, $\bar{\gamma}_2$ for both DSTC and DBF modes of communications for various values of M. In all scenarios/cases assumed, the performance improves as M increases, with a decreased, however, rate. In the same figure, the high SNR asymptotic results are also included and prove their tightness even for moderate values of $\bar{\gamma}_2$ (as are the ones employed in this figure), when compared with Monte Carlo simulations and the exact results.

2) Power Consumption Optimization: We will now discuss the optimization of the UAV transmit power that has been presented in II.C.4. Specifically, we will analyze the dependence of the total UAV power consumption with the total number K of UAVs present, while keeping the OP fixed to a predefined target. To clearly showcase this dependence, and without loss of generality, we will assume that all UAVs correctly decode the message from the first communication phase. We will only provide details for the case of DSTC (since DBF will have a similar behavior). From expression (2), naively one would expect that the total power is an increasing function of K. However, as seen in Fig. 4, the total UAV power consumption vs K initially is a decreasing function before it starts increasing. To understand this non-monotonic behavior, we start by noting that for large SNR, the outage of the highest M SNRs out of K scales with K, roughly as $P_{\text{out}} \sim 1/(MP_r)^{mL_dK}$, as seen also in (17). As a result, $MP_r \sim (P_{\text{out}})^{(mL_dK)^{-1}}$, and hence it is a decreasing function of K, and in fact for small K substantially so. Thus, as seen in Fig. 4, the total UAV power consumed appearing in (2) initially decreases and then eventually increases with K. The minimum is increasing with M, mainly due to the fact that the transmitting circuits power expenditure increases with M. Since power consumption is an important factor for the satisfactory operation of the UAV-enabled communication networks, this analysis shows that a relatively small number K of available UAVs is sufficient to achieve an excellent compromise among performance and power consumption. It is noteworthy that similar outcomes can be obtained by employing other SNR-based performance criteria, e.g., BER.

[4]It is noted that $m = 1$ corresponds to Rayleigh fading conditions.

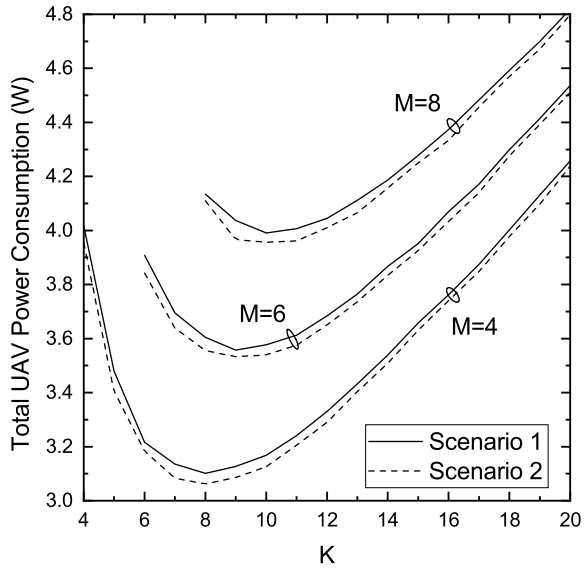

Fig. 4. Total UAV power consumption vs. K ($G_T = G_R = 6$dB, $d_D = 1000$m, $h = 70$m, $\alpha_{rd} = 2.5$, $\alpha_{sd} = 3.2$). P_r is obtained by fixing the OP to $p^* = 10^{-2}$.

IV. Scenario 2: Dual One/Two Hop Communications

In this scenario, the direct link between the S and the D is assumed to be occasionally available. As discussed in the previous scenario, there are two phases of communications. In the first one, the transmitted message can be received by both the D and the UAVs. Since the UAVs are much closer to S, compared to D, it is reasonable to assume that the message is always received successfully by all K UAVs, and hence we will not further analyze this leg. The SNR of the direct path can be expressed as

$$\mathrm{SNR}_{\mathrm{sd}} = \overline{\gamma}_{\mathrm{sd}} \sum_{\ell=1}^{L_s} \sum_{n=1}^{L_d} x_{\ell n}, \tag{39}$$

where $x_{\ell n}$ is the normalized modulus square of the channel coefficient between source antenna ℓ and destination antenna n. The quantities $x_{\ell n}$ are assumed i.i.d. following the Nakagami-m distribution, with PDF given in (1), for $\Omega = 1$. The mean SNR coefficient $\overline{\gamma}_{sd}$ is given by

$$\overline{\gamma}_{\mathrm{sd}} = \frac{P_t}{N_0} \left(\frac{G_T G_R \lambda^2}{16\pi^2 d_{sd}^{a_{sd}}} \right). \tag{40}$$

As a result, the CDF of SNR_{sd}, $F_{\mathrm{sd}}(x)$, is given by [36]

$$F_{\mathrm{sd}}(x) = \gamma \left(mL_s L_d, \frac{mx}{\overline{\gamma}_{\mathrm{sd}}} \right). \tag{41}$$

When the message is not successfully received at D, i.e., if $\mathrm{SNR}_{\mathrm{sd}} < \gamma$, where γ denotes a predefined threshold, the second communication phase commences, during which the UAVs retransmit the decoded packet they have received. We assume that the signals between the UAVs and S are perfectly synchronized. For simplicity, we assume only open-loop transmission. In summary, the total received SNR at D, over both communication phases, can be expressed as

$$\mathrm{SNR}_{3,\mathrm{tot}} = \begin{cases} \mathrm{SNR}_{\mathrm{sd}}, & \mathrm{SNR}_{\mathrm{sd}} \geq \gamma \\ \mathrm{SNR}_{\mathrm{sd}} + \mathrm{SNR}_{2,\mathrm{st}}, & \mathrm{SNR}_{\mathrm{sd}} < \gamma, \end{cases} \tag{42}$$

where $\mathrm{SNR}_{2,\mathrm{st}}$ is the received SNR from the 2nd leg of communications from the UAVs to D given in (13). Hence, since all UAVs have correctly decoded the received signal, the binomial summation in (38) only contains one term ($N = K$ and thus $M_N = M$) and the OP for this scenario can be expressed as

$$\begin{aligned} P_{\mathrm{out}} = F_{3,\mathrm{st}}^{M,K}(\gamma) &= \mathbb{P}\left(\mathrm{SNR}_{\mathrm{sd}} < \gamma, \mathrm{SNR}_{\mathrm{tot}} < \gamma\right) \\ &= \mathbb{P}\left(\mathrm{SNR}_{\mathrm{tot}} < \gamma\right). \end{aligned} \tag{43}$$

The above probability may be evaluated explicitly in the following.

Proposition 4.1: (Scenario 2: Exact Outage $F_{3,\mathrm{st}}^{M,K}(\gamma)$ for DSTC): The OP of the scheme under consideration can be expressed as, (44), shown at the bottom of the next page, with $\mathcal{D}_1 = \frac{\left(\frac{m}{\overline{\gamma}_2}\right)^{k_1+mL_d}\binom{k_1}{k_2}(-1)^{k_2}}{k_1!\Gamma(mL_d)}$, $\mathcal{D}_2 = \mathcal{D}_1\left(1+\frac{i_M}{M}\right)^{k_1}\left(\frac{\overline{\gamma}_2}{\overline{\gamma}_{\mathrm{sd}}}\right)^{mL_d}$,

$$\mathcal{D}_3(y) = \Gamma\left(mL_d + k_2\right) \frac{\gamma\left(mL_d + k_2, \left(\frac{m}{\overline{\gamma}_{\mathrm{sd}}} - \frac{m}{\overline{\gamma}_2} y\right) x\right)}{\left(\frac{m}{\overline{\gamma}_{\mathrm{sd}}} - \frac{m}{\overline{\gamma}_2} y\right)^{k_2+mL_d}},$$

while $f_1(x) = x^{k_1-k_2} \exp\left(-\frac{m}{\overline{\gamma}_2} x\right)$ *and* $f_2(x) = x^{k_1-k_2} \exp\left(-\frac{m(M-i_M)}{M\overline{\gamma}_2} x\right)$.

Proof: The proof can be found in Appendix D. ∎

Corollary 4.1: (Scenario 2: High SNR Outage $F_{3,\mathrm{st}}^{M,K}(\gamma)$ for DSTC): In the limit of $\gamma \ll \bar{\gamma}_2$ it can be shown that

$$\begin{aligned} F_{3,\mathrm{st}}^{M,K}(\gamma) \approx \mathcal{H} &\left(\frac{m}{\overline{\gamma}_2}\right)^{mL_dK+mL_d^2} \\ &\cdot \frac{\gamma^{mL_d^2+mL_dK+1} B_1\left(mL_d^2+1, mL_dK+1\right)}{\Gamma(mL_dK+1)\Gamma(mL_d^2+1)}. \end{aligned} \tag{45}$$

In an effort to further simplify the results presented above and using the asymptotic approximation discussed in the previous section, we show in Appendix C that the OP can be expressed as follows:

Proposition 4.2: (Scenario 2: Outage $F_{3,\mathrm{st}}^{M,K}(\gamma)$ for DSTC: $M < K$): Assume $\beta < 1$ and $\lambda_s = L_d/K$ and let

$$\begin{aligned} \overline{Q}_{3,\mathrm{st}}^{M,K}(z) = &\frac{\sqrt{\beta}}{y_0\sqrt{(1-\beta)|\phi_{yy}|}} \\ &\cdot e^{K\left[\phi(y_0,s_0;z)+\frac{1}{2}s_0^2\left(\phi_{ss}-\frac{\phi_{ys}^2}{\phi_{yy}}\right)\right]} \\ &Q\left(\sqrt{Ks_0^2\left(\phi_{ss}-\frac{\phi_{ys}^2}{\phi_{yy}}\right)}\right). \end{aligned} \tag{46}$$

Then let

$$\overline{P}_{3,\mathrm{st}}^{M,K}(z) = \begin{cases} \overline{Q}_{3,\mathrm{st}}^{M,K}(z) & \text{if } z < z_{erg} \\ 1 - \overline{Q}_{3,\mathrm{st}}^{M,K}(z) & \text{if } z > z_{erg}, \end{cases} \tag{47}$$

where

1) $\phi(y, s; z)$ *is given by*

$$\phi(y,s;z) = \beta z s + (1-\beta)\log\left[\frac{\gamma\left(mL_d, \frac{t(y)}{1+s}\right)}{1-\beta}\right]$$

$$+\beta \log\left(\frac{y}{\beta}\right) - \beta m L_d \log(1+s) - m L_d \lambda_s \log(1+s\frac{\overline{\gamma}_{sd}}{\overline{\gamma}_2}),$$

2) y_0, s_0 *are the solutions of the fixed point equations*

$$\frac{\partial \phi}{\partial y} = \frac{\partial \phi}{\partial s} = 0 \tag{48}$$

3) $\phi_{yy}, \phi_{ys}, \phi_{ss}$ *are the second partial derivatives of* ϕ *with respect to the indices (i.e.,* $\phi_{yy} = \frac{\partial^2 \phi}{\partial y^2}$*, etc.), evaluated at* y_0, s_0*, and*

4) z_{erg} *is the solution of* (48) *setting* $s = 0$ *and corresponds to the most probable value of the asymptotic distribution.*

Then, for every $z > 0$ *the CDF of the normalized value of SNR$_{tot}$ converges to* $\overline{P}_{3,\mathrm{st}}^{M,K}(z)$ *in the sense*

$$\lim_{K\to\infty} K \left| F_{3,\mathrm{st}}^{M,K}\left(\frac{\overline{\gamma}_2 M z}{m}\right) - \overline{P}_{3,\mathrm{st}}^{M,K}(z) \right| < \infty. \tag{49}$$

Proof: The proof follows the lines of 3.3 in App. V, by multiplying the MGF $\overline{M}_{2,\mathrm{st}}^{M,K}(s)$ in (A-1) by $(1 + s\bar{\gamma}_{\mathrm{sd}}/\overline{\gamma}_2)^{-mL_sL_d}$, which is the MGF of $F_{\mathrm{sd}}(\gamma)$. ■

The above expressions simplify when $M = K$:

Proposition 4.3: (Scenario 2: Outage $F_{3,\mathrm{st}}^{M,M}(\gamma)$ *for DSTC:* $M = K$*): Let* $\lambda_s = L_d/M > 0$ *and*

$$\overline{Q}_{3,\mathrm{st}}^{M,M}(z) = e^{M\left[\phi(s_0;z)+\frac{1}{2}s_0^2\phi_{ss}\right]} Q\left(\sqrt{M s_0^2 \phi_{ss}}\right), \tag{50}$$

and let

$$\overline{P}_{3,\mathrm{st}}^{M,M}(z) = \begin{cases} \overline{Q}_{3,\mathrm{st}}^{M,M}(z) & \text{if } z < z_{erg} \\ 1 - \overline{Q}_{3,\mathrm{st}}^{M,M}(z) & \text{if } z > z_{erg}, \end{cases} \tag{51}$$

where

1) $\phi(s;z)$ *is given by*

$$\phi(s;z) = zs - mL_d\left(\log(1+s) - \lambda_s \log(1+\frac{s\overline{\gamma}_{sd}}{\overline{\gamma}_2})\right), \tag{52}$$

2) s_0 *is the solution of the fixed point equation* $\frac{\partial \phi}{\partial s} = 0$.

3) z_{erg} *is the solution of the saddle point equation* $\frac{\partial \phi}{\partial s} = 0$*, setting* $s = 0$ *and corresponds to the most probable value of the asymptotic distribution.*

Then, for every $z > 0$ *the CDF of the normalized value of SNR$_{tot}$ converges to* $\overline{P}_{3,\mathrm{st}}^{M,M}(z)$ *in the sense*

$$\lim_{M\to\infty} M \left| F_{3,\mathrm{st}}^{M,M}\left(\frac{\overline{\gamma}_2 M z}{m}\right) - \overline{P}_{3,\mathrm{st}}^{M,M}(z) \right| < \infty. \tag{53}$$

A. Performance Analysis of Scenario 2

We will now use the above analytical results for the two legs of communication to quantify the performance of the full link.

1) End-to-End Outage Probability: In Scenario 2, we have assumed that all UAVs receive the packet perfectly in the first leg of communication. As a result, we have $\Pi_N = \delta_{N,K}$ in (9), and hence the total OP is given by (43). In Fig. 5a, the E2E OP is plotted as a function of the transmission rate R for both scenarios under investigation including the benchmark direct path. It is clear that Scenario 2 offers considerable improvement on the OP performance, which is made possible from taking advantage the intermittent existence of the direct link. Moreover, we observe in all cases the tightness of the proposed asymptotic results.

2) Goodput: When comparing the performance of the one-hop direct link between S and D with that of the two-hop link using the UAVs, one has to note that even though the coding rate is the same in both cases, the overall throughput rate is not. This is so because in the two hop link, the number of bits received per channel use is half, since the time needed is double. As a result, a direct link with even a moderate outage performance can increase the amount of data sent significantly, even when the two-hop link can achieve a low outage, as we have seen. To quantify this effect, we use the so-called goodput criterion, defined as the average number of bits received in the combined link over long periods of time. In this case the goodput can be expressed as

$$\bar{R} = R\,\mathbb{P}(\mathrm{SNR}_{\mathrm{sd}} > \gamma_R) + \frac{R}{2}\,\mathbb{P}(\mathrm{SNR}_{\mathrm{sd}} < \gamma_R, \mathrm{SNR}_{\mathrm{tot}} > \gamma_R). \tag{54}$$

In the above equation the first term is the goodput of the direct link, while the second is the additional gain in bits from the existence of the relay link. The goodput of the 2-hop relay link corresponding to the first scenario takes the simpler form

$$\bar{R} = \frac{R}{2}\,\mathbb{P}(\mathrm{SNR}_{2,\mathrm{st}} > \gamma_R). \tag{55}$$

$$\begin{aligned} F_{3,\mathrm{st}}^{M,K}(\gamma) = \mathcal{C}_1 &\left[\bar{F}_2\left(\frac{m\gamma}{\bar{\gamma}_{sd}}\right) - \widetilde{\sum_{k_1,k_2}} \mathcal{D}_1\mathcal{D}_3(1) f_1(\gamma)\right] \\ &+ \sum_{\substack{i_{1\sim M} \\ n_i}} \mathcal{B}\Gamma(k+1) \\ &\cdot \left[\mathcal{C}_2\left(\bar{F}_2\left(\frac{m\gamma}{\bar{\gamma}_{\mathrm{sd}}}\right) - \widetilde{\sum_{k_1,k_2}} \mathcal{D}_2\mathcal{D}_3\left(\frac{M+i_M}{M}\right) f_2(\gamma)\right)\right. \\ &\left. + \mathcal{C}_3\left(\bar{F}_2\left(\frac{m\gamma}{\bar{\gamma}_{\mathrm{sd}}}\right) - \widetilde{\sum_{k_1,k_2}} \mathcal{D}_1\mathcal{D}_3\,(1)\, f_2(\gamma)\right)\right], \end{aligned} \tag{44}$$

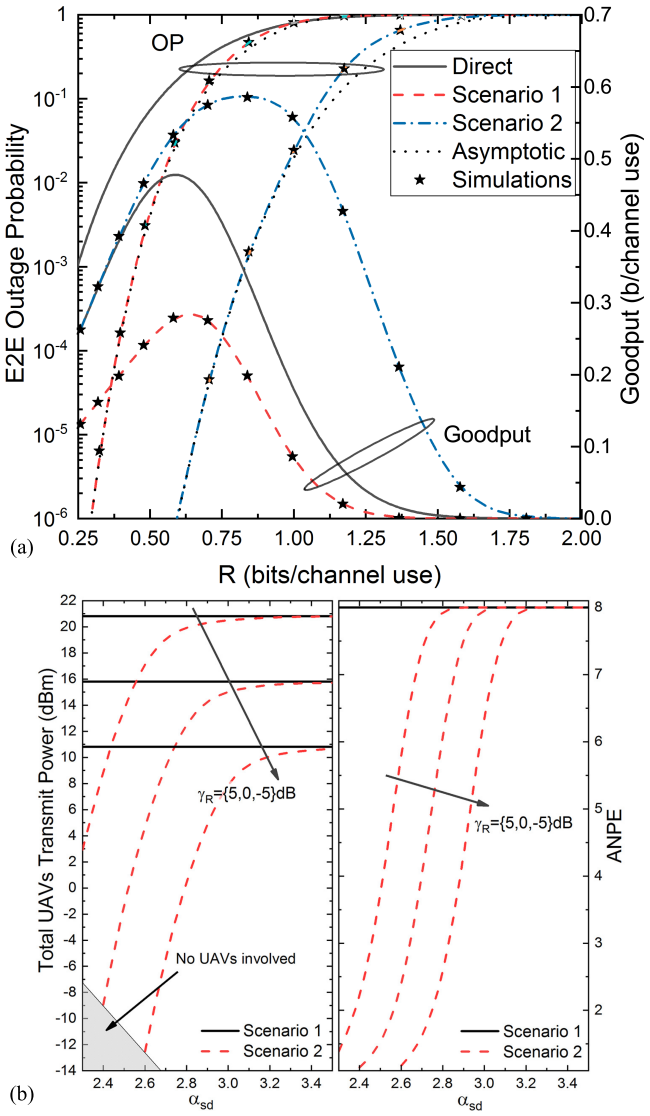

Fig. 5. (a) E2E OP and Goodput vs. R for the 2 scenarios under investigation (P_t =4dBm, P_r = 0dBm, $L_s = L_d = 2$). Direct S-D communications outperforms Scenario 1 in terms of goodput. (b) Total UAV transmit power and ANPE vs. a_{sd} for various values of γ_R (P_t =5dBm, $\alpha_{rd} = 2.4$, $L_s = L_d = 2$). The number of UAVs employed increases as path loss exponent increases.

In Fig. 5a, we also plot on the right y-axis the goodput for the direct link as well as the two scenarios proposed. Interestingly, while the outage of the direct link is poor relative to the relayed paths of outage performance of the direct link, it provides a significant gain in goodput as compared to Scenario 1.

3) Power Consumption: The behavior of the UAV power consumption as a function of K, i.e., the number of UAVs present, is very similar in this scenario as in Scenario 1, as it is depicted in Fig. 4. The only difference here is that UAV power transmission is active (i.e., $P_r > 0$), only when the direct link between S and D is not possible. As a result, we need to replace P_r in (2) with $P_r F_{\rm sd}(\gamma_R)$.

4) Signalling Overhead: The signalling overhead for the schemes under consideration can be quantified using the criterion of ANPE. In the case of Scenario 1, since all available UAVs are always employed in the 2nd leg of communications, the ANPE can be evaluated as $N_1(\gamma_R) = \bar{N}(\gamma_R) L_d$ where

$$\bar{N}(\gamma_R) = \sum_{N=1}^{K} \Pi_N(\gamma_R) \cdot N, \tag{56}$$

and Π_N is given by (9). In contrast, in Scenario 2, the ANPE takes the form

$$N_2(\gamma_R) = L_s L_d \left(1 - F_{\rm sd}(\gamma_R)\right) + F_{\rm sd}(\gamma_R) \bar{N}(\gamma_R) L_d. \tag{57}$$

From (57), it is evident that the average number of UAVs employed is related to the channel conditions of the direct link as well as the Scenario's 2 predefined threshold.

In Fig. 5b, in an effort to quantify the impact of the direct link to the system's performance, the total transmit power of the relays, as it is defined in IV-A.3, is plotted as a function of the path loss factor of the direct link α_{sd}, for both scenarios under investigation and various values of the outage threshold γ_R. It is shown that as α_{sd} increases, i.e., the propagation conditions of the direct link deteriorate, the required total transmit power of the UAVs for Scenario 2 approaches the corresponding one of Scenario 1. The reason is that due to the unfavorable channel conditions for the direct link, the algorithm in Scenario 2 obliges more relays to be involved in the communication, as it is shown by the investigation of the ANPE that is plotted in the right subfigure of Fig. 5b. It is interesting to be noted that for low values of α_{sd} the OP target has been achieved without requiring to employ UAVs in the communications.

V. Discussion - Outlook

In closing, this analysis has reaffirmed the potential of UAVs acting as relays to improve the communication link between two nodes. We have considered two scenaria: In the first, there is no direct link available between S and D. Transmission occurs in two stages, first from the S to the K UAVs hovering on top, and second from the UAVs that decoded the message to the D. In the second stage, a generalized selection methodology is applied, in which only a subset of M UAVs with the highest link quality to the D participate in the transmission. The second, hybrid, scenario allows for the possibility of an intermittent direct link. In this case, the first stage takes place as above, but the second stage takes place only if the receiver at D has not decoded the packet through the direct link. Nevertheless, we have found that in the presence of even a relatively bad direct link, the goodput of the system increases, due to the corresponding skipping of the second communication stage. While the benefits from pathloss gains due to the heightened location of UAVs has long been addressed, in this paper we have provided an assessment of the improvement of the communication link by enlarging the spatial footprint of the intermediate UAV link through UAV cooperation.

Subject to the availability of CSI at the UAVs, two cooperating transmission schemes have been analyzed. Specifically, in its absence, a DSTC scheme is proposed over the M transmitting UAVs, providing significant diversity and power gains compared to a single UAV present. In contrast, when timely

CSI is available, then it is optimal for the UAVs to transmit in a coherent manner, through DBF. In this case, DBF performance out-competes DSTC, providing consistently an M-fold increase in the outage SNR. The challenge of conveying CSI to UAVs, with the necessity of UAV information exchange, can be overcome using slave-master methods, which also allows for synchronization between the UAV clocks [48]. The optimal number of available UAVs K can be obtained using a number of metrics. For example, the total UAV communications power, evaluated at a fixed outage, surprisingly has a well-defined minimum as a function of K, and thus can be used as such a metric. The optimal maximum number of UAVs simultaneously used, M, can be determined by other criteria. For example, if M is too large, then the space-time codeword becomes too long for tracking the channel inbetween pilots, when compared with the Doppler spread. Further, the complexity of the DSTC may become too high to be employed in a distributed fashion.

Furthermore, we have used a number of mathematical tools to obtain the OP. While we have obtained exact expressions for the DSTC OP, we have also calculated easy-to-use, asymptotic, closed-form expressions for both DSTC and DBF OPs, proposing a novel method based on the saddle-point approach. The expressions are valid for asymptotically large UAV numbers, but work quite accurately even for few UAVs. In closing, we note that there are several open challenges that need to be addressed to make the use of UAVs as relays viable. One challenge includes the impact of synchronization and random frequency offset errors on SBF [49]. Furthermore, it would be quite important to exploit UAVs as a large antenna to transmit multiplexed information to multiple separate destinations, in which case distributed multiple-input multiple output techniques will be necessary. Additionally, the UAV-selection criterion could also take into account energy efficiency constraints for extending the applicability of the proposed approach, Finally, since in many UAV-enabled communication scenarios the impact of shadowing cannot be neglected, it is very important to extend the analytical results in order to investigate such scenarios.

Appendix A Proof of Proposition 3.1

In this appendix, we will prove Proposition 3.1, obtaining the OP $F_{2,\mathrm{st}}^{M,N}(x)$, i.e., the CDF of $\mathrm{SNR}_{2,\mathrm{st}}$, defined in (13), which involves the sum of the M highest values out of N random variables from a Nakagami-mL_d distribution, for $M < N$. The definition of the OP appears in (14). It is convenient to work with a normalized random variable $Z = \frac{m\mathrm{SNR}_{2,\mathrm{st}}}{M\overline{\gamma}_2}$. Starting from (14), the MGF (Laplace transform) of Z can be expressed as [40, eq. (5)]

$$\begin{aligned}\overline{M}_{2,\mathrm{st}}^{M,N}(s) &= \mathbb{E}_Z\left[e^{-sMZ}\right] \\ &= M\binom{N}{M}\int_0^\infty dx\, x^{mL_d-1}e^{-x(1+s)}\gamma(mL_d,x)^{N-M} \\ &\quad\cdot\left(\frac{1-\gamma(mL_d,x(1+s))}{(1+s)^{mL_d}}\right)^{M-1}. \end{aligned} \tag{A-1}$$

From the above expression, the PDF and CDF of Z are, respectively, given by

$$\begin{aligned} f_Z(z) &= M\int\frac{ds}{2\pi}e^{Msz}\overline{M}_{2,\mathrm{st}}^{M,N}(s), \\ F_Z(z) &= \int\frac{ds}{2\pi}e^{Msz}\frac{\overline{M}_{2,\mathrm{st}}^{M,N}(s)}{s}, \end{aligned} \tag{A-2}$$

with the integrals over s being along the imaginary axis, corresponding to the inverse Laplace transform. Then $F_{2,\mathrm{st}}^{M,N}(\gamma)$ can be expressed as follows:

$$F_{2,\mathrm{st}}^{M,N}(x) = F_Z\left(\frac{mx}{M\overline{\gamma}_2}\right). \tag{A-3}$$

In order to evaluate (A-1), we expand the $\gamma(mL_d,x)^{N-M}$ as follows

$$\begin{aligned}\gamma\left(mL_d,x\right)^{N-M} &\overset{(1)}{=} \left(1-e^{-x}\sum_{j=0}^{mL_d-1}\frac{x^j}{j!}\right)^{N-M} \\ &\overset{(2)}{=} \sum_{i_M=0}^{N-M}\binom{N-M}{i_M}e^{-i_Mx}\left(-\sum_{j=0}^{mL_d-1}\frac{x^j}{j!}\right)^{i_M} \\ &\overset{(3)}{=} \sum_{i_M=0}^{N-M}\binom{N-M}{i_M}(-1)^{i_M}e^{-i_Mx} \\ &\quad\cdot\sum_{\substack{n_1=0\\ n_1+n_2+\cdots+n_{mL_d}=i_M}}^{i_M}\sum_{n_2=0}^{i_M}\cdots\sum_{n_{mL_d}=0}^{i_M} i_M!\prod_{j=1}^{L_dm}\frac{x^{(j-1)n_j}}{n_j!\left((j-1)!\right)^{n_j}}, \end{aligned} \tag{A-4}$$

where (1) holds due to [30, eq. (8.352/1)], (2) holds due to binomial identity, and (3) holds due to [50, eq. (24.1.2)]. Moreover, the following expansion is also employed

$$\begin{aligned}&\frac{1-\gamma\left(L_dm,(1+s)x\right)}{(1+s)^{L_dm}} \\ &\quad\overset{(1)}{=}\sum_{i_1=0}^{mL_d-1}\frac{x^{i_1}(1+s)^{-L_dm+i_1}e^{-x(1+s)}}{i_1!}, \end{aligned} \tag{A-5}$$

where (1) is due to [30, eq. (8.352/2)]. After expanding the corresponding expression $M-1$ times and finally integrating over x we obtain the following closed-form expression for the MGF of Z, composed of simple and easy-to-evaluate functions,

$$\begin{aligned}\overline{M}_{2,\mathrm{st}}^{M,N}(s) &= \sum_{i_{1\sim M}}\mathcal{A}\left(1+s\right)^{i_{M-1}-(M-1)mL_d} \\ &\quad\cdot\left(s+\frac{M+i_M}{M}\right)^{-mL_d-i_{M-1}-S_M}, \end{aligned} \tag{A-6}$$

where

$$\sum_{\substack{i_{1\sim M}\\ n_i}} = \sum_{i_{1\sim M}}\cdot\sum_{n_i} = \sum_{i_1=0}^{mL_d-1}\sum_{i_2=0}^{mL_d+i_1-1}\cdots\sum_{i_{M-1}=0}^{mL_d+i_{M-2}-1}$$

$$\cdot \sum_{i_M=0}^{N-m} \sum_{n_1=0}^{i_M} \sum_{n_2=0}^{i_M} \cdots \sum_{n_{mL_d}=0}^{i_M} \tag{A-7}$$
$$n_1+n_2+\cdots+n_{mL_d}=i_M$$

$$\mathcal{A} = \frac{N!(-1)^{i_M} M^{-p_1-i_{M-1}}}{(N-M-i_M)!} \left(\prod_{\substack{j=1 \\ i_0=0}}^{M-1} \frac{j^{i_j-i_{j-1}-mL_d}}{i_j!} \right) \cdot \left(\prod_{j=1}^{M-2} \Gamma(mL_d+i_j) \right) \left(\prod_{j=1}^{M} \frac{1}{n_j!((j-1)!)^{n_j}} \right) \tag{A-8}$$

$$\mathcal{B} = \mathcal{A} M^{q_2-S_M} \frac{\Gamma(p_1)}{\Gamma(p_M)} i_M^{1-p_M} \frac{\Gamma(p_M-1)}{\Gamma(q_1)} (1-p_M)_{q_1}.$$

Therefore, (A-6) is now in appropriate form to be used for evaluating the corresponding PDF expression, by employing the inverse Laplace transform and using [51, eq. (2.1.2/71)], resulting to

$$f_{2,\mathrm{st}}^{M,N}(x) = \sum_{i_{1\sim M}} \frac{\mathcal{A}}{\overline{\gamma}_2^{p_M}} \frac{m^{p_M} x^{p_M-1}}{\Gamma(p_M)} \exp\left(-\frac{m}{\overline{\gamma}_2} x\right) \cdot {}_1F_1\left(i_{M-1}+p_1; p_M; -\frac{m i_M}{M\overline{\gamma}} x\right), \tag{A-9}$$

where ${}_1F_1(\cdot)$ denotes the confluent hypergeometric function [30, eq. (9.210/1)]. Moreover, based also in (A-6), (A-2) and [51, eq. (2.1.3/1)], the following expression is deduced

$$F_{2,\mathrm{st}}^{M,N}(x) = \sum_{i_{1\sim M}} \frac{\mathcal{A}}{\overline{\gamma}_2^{p_M}} \frac{(mx)^{p_M}}{\Gamma(p_M+1)} \cdot \Phi_2\left(q_1, p_1, p_M+1, -\frac{m}{\overline{\gamma}_2} x, -\frac{m(M+i_M)}{M\overline{\gamma}_2} x\right), \tag{A-10}$$

where $\Phi_2(\cdot)$ denotes the confluent hypergeometric function of two variables [30, eq. (9.261/1)]. A simpler closed-form expression can be derived based on the PDF provided in (A-9) and using a finite series representation for the confluent hypergeometric function [52, eq. (07.20.03.0024.01)] resulting to (16).

Appendix B Proof of Corollary 3.1

In this appendix, the analytical steps for deriving the asymptotic expression of $F_{2,\mathrm{st}}^{M,N}(\gamma)$, when $\gamma/\bar{\gamma}_2 \ll 1$ which appears in Corollary 3.1. We start by noting that this limit corresponds to the small $z \ll 1$ limit in (A-2), which in turn corresponds to the large s-limit in (A-1). After changing variables from x to $x/(1+s)$ and taking the large s limit, we obtain

$$\overline{M}_{2,\mathrm{st}}^{M,N}(s) \approx M \frac{\Gamma(mL_d+1)^{M-N}}{(1+s)^{mL_dN}} \binom{N}{M} \cdot \int_0^\infty dx \frac{x^{(mL_d-1)(N+1-M)} e^{-x}}{\Gamma(mL_d)} \left(1-\gamma(mL_d,x)\right)^{M-1}. \tag{B-1}$$

Expanding the product of incomplete Gamma functions as in (A-5) and integrating over x, while also performing the inverse Laplace transform as in (A-5) results to

$$F_{2,\mathrm{st}}^{M,N}(\gamma) \approx \mathcal{H} \left(\frac{m\gamma}{\overline{\gamma}_2}\right)^{mL_dN}, \tag{B-2}$$

which is (17) with $\mathcal{H}$ appearing in (18).

Appendix C Proof of Proposition 3.2

We start with the MGF of the random variable $Z = \frac{m\mathrm{SNR}_{2,\mathrm{st}}}{M\overline{\gamma}_2}$ appearing in (A-1). Changing variables to $t = x(1+s)$ and $y = 1-\gamma(mL_d, t)$ and using the Stirling approximation for the factorial function

$$\log N! = N\log N - N + \log\sqrt{2\pi N} + O(N^{-1}) \tag{C-1}$$

the probability distribution of z takes the form

$$\overline{f}_{2,\mathrm{st}}^{M,N}(z) = \frac{M^2}{\sqrt{2\pi N\beta(1-\beta)}} \int_{-i\infty}^{i\infty} \frac{ds}{2\pi i} \int_0^1 \frac{dy}{y} e^{N\phi(y,s;z)}, \tag{C-2}$$

where $\phi(\cdot)$ appears in (21). Keeping in mind that in the large N limit $\phi(\cdot) = O(1)$, we proceed to integrate over s and y. Since for $\mathcal{R}e(s) > -1$ ϕ is analytic in s, we deform the contour of the s-integral to pass through the saddle point of $\phi(y,s;z)$, from the steepest descent path [41], which is defined by the equations (22):

$$\frac{\beta}{y} = \frac{1-\beta}{\gamma\left(mL, \frac{t}{1+s}\right)} \frac{e^{\frac{ts}{1+s}}}{(1+s)^{mL}},$$
$$\beta z = \left(\frac{t}{1+s}\right)^{mL} \frac{(1-\beta)e^{-\frac{t}{1+s}}}{\gamma\left(mL, \frac{t}{1+s}\right)\Gamma(mL)(1+s)} + \frac{\beta mL}{1+s}. \tag{C-3}$$

The above equations can only have real solutions for s and y in the region $\mathcal{R}e(s) > -1$, and due to monotonicity it can be shown to be unique. For large N the integral will be dominated by the behavior close to the saddle point. As a result, we may expand the exponent close to s_0, y_0. Thus

$$\phi(y,s;z) = \phi(y_0,s_0;z) + \frac{\delta\mathbf{x}^T}{2} \begin{pmatrix} \phi_{yy} & \phi_{ys} \\ \phi_{ys} & \phi_{ss} \end{pmatrix} \delta\mathbf{x} + O(\delta\mathbf{x}^3), \tag{C-4}$$

where $\delta\mathbf{x} = [y-y_0, s-s_0]^T$ and ϕ_{yy} etc, are the second partial derivatives of ϕ with respect to their indices evaluated at the saddle point. Keeping at the exponent up to the quadratic terms and expanding the rest, we are left with a quadratic integral, which can be integrated along the stationary phase lines, resulting to

$$\overline{f}_{2,\mathrm{st}}^{M,N}(z) = \frac{\beta^2\sqrt{N}}{\sqrt{2\pi\beta(1-\beta)}} \frac{e^{N\phi(y_0,s_0;z)}}{\sqrt{\phi_{sy}^2 - \phi_{yy}\phi_{ss}}} \left(1+O(N^{-1})\right). \tag{C-5}$$

The leading correction $O(N^{-1})$ originates from three terms. The first is the correction to the Stirling approximation of the factorials, which we have already seen. The second originates from a perturbation term proportional to $N\delta\mathbf{x}^4$ from the expansion of the quartic term in $\delta\mathbf{x}$ from the exponential.

$$\mathcal{I}_3 = \Gamma(n_2)\left[\frac{\gamma\left(n_1, A_1\gamma\right)}{A_1^{n_1}} - \exp\left(-A_2\gamma\right) \cdot \widetilde{\sum_{k_1,k_2}} \binom{k_1}{k_2} \frac{A_2^{k_1}\gamma^{k_1-k_2}(-1)^{k_2}}{k_1!(A_1-A_2)^{k_2+n_1}} \gamma\left(k_2+n_1, (A_1-A_2)\gamma\right)\right], \tag{D-4}$$

Integrating over $\delta\mathbf{x}$ makes this term $O(N^{-1})$. There is another correction proportional to $N^2\delta\mathbf{x}^6$, which originates from quadratic expansion of the cubic term in the exponent, which also gives a correction at the same order. As a result, we have that the above approximation to the PDF of z is valid to order $O(N^{-1})$.

As far as the CDF is concerned, we will deal only with the case $z < z_{erg}$, since the opposite case $z > z_{erg}$ can be analyzed in a similar way. $\overline{P}_{2,\mathrm{st}}^{M,N}(z)$ is defined as

$$\overline{P}_{2,\mathrm{st}}^{M,N}(z_0) = \int_0^{z_0} \overline{f}_{2,\mathrm{st}} M, N(z) dz. \tag{C-6}$$

The analysis is based on the fact that for large N the CDF is determined from the behavior of $\overline{f}_{2,\mathrm{st}}^{M,N}(z)$ close to $z = z_0$. Hence we expand ϕ close to z_0 to second order

$$\phi(y, s; z) = \phi(y_0, s_0; z_0) + \dot{\phi}_0(z - z_0) + \frac{1}{2}\ddot{\phi}_0(z - z_0)^2 + \ldots, \tag{C-7}$$

where $\dot{\phi}_0$ and $\ddot{\phi}_0$ are the first and second (total) derivatives of ϕ evaluated at z_0, which can be obtained to be $\dot{\phi} = \beta s_0, \ddot{\phi} = -\frac{\beta^2\phi_{yy}}{\phi_{yy}\phi_{ss}-\phi_{ys}^2}$. Hence, after integrating the above quadratic expansion over z we get (20), while (23) follows from the fact that the corrections are $O(N^{-1})$.

Appendix D Proof of Proposition 4.1

In this appendix, the evaluation of $F_{3,\mathrm{st}}^{M,N}(\gamma)$ is presented. Since an outage event occurs when $\mathrm{SNR}_{3,\mathrm{tot}} = \mathrm{SNR}_{\mathrm{sd}} + \mathrm{SNR}_{2,\mathrm{st}} < \gamma$, we may express the above OP as a convolution

$$F_{3,\mathrm{st}}^{M,N}(\gamma) = \int_0^{\gamma} F_{2,\mathrm{st}}^{M,N}(\gamma - x) F'_{sd}(x) dx, \tag{D-1}$$

where $F'_{sd}(x)$ is the derivative of $F_{sd}(x)$ appearing in (41). Substituting (16) and (41), integrals of the following form appear

$$\mathcal{I}_3 = \int_0^{\gamma} \gamma_1^{n_1-1} \exp\left(-A_1\gamma_1\right) \gamma\left(n_2, A_2\left(\gamma - \gamma_1\right)\right) d\gamma_1, \tag{D-2}$$

where $\{n_1, n_2\} \in \mathbb{Z}^+$, $\{A_1, A_2\} \in \mathbb{R}^+$, with $A_1 \neq A_2$. Using the finite series expansion and the definition of the lower incomplete gamma function, i.e., [30, eqs. (8.352/1 and 8.350/1)], (D-2) is expressed as

$$\mathcal{I}_3 = \Gamma(n_2)\left[\frac{\gamma\left(n_1, A_1\gamma\right)}{A_1^{n_1}} - e^{-A_2\gamma} \cdot \sum_{k_1=0}^{n_2-1} \int_0^{\gamma} \frac{\left(A_2(\gamma-\gamma_1)\right)^{k_1}}{k_1!} \gamma_1^{n_1-1} e^{-(A_1-A_2)\gamma_1} d\gamma_1\right]. \tag{D-3}$$

Moreover, using the binomial identity in (D-3), [30, eq. (8.350/1)] and after some mathematical manipulation, yields to the following closed-form expression, (D-4), as shown at the top of the page, where $\widetilde{\sum_{k_1,k_2}} = \sum_{k_1=0}^{n_2-1}\sum_{k_2=0}^{k_1}$. Using the above solution and after some mathematical simplifications finally yields (44) and completes this proof.

Acknowledgment

The authors acknowledge useful discussions with Dr. Andreas Polydoros at the initial stages of this work.

References

[1] X. Cao, P. Yang, M. Alzenad, X. Xi, D. Wu, and H. Yanikomeroglu, "Airborne communication networks: A survey," *IEEE J. Sel. Areas Commun.*, vol. 36, no. 10, pp. 1907–1926, Sep. 2018.

[2] Z. Yuan, J. Jin, L. Sun, K.-W. Chin, and G.-M. Muntean, "Ultra-reliable IoT communications with UAVs: A swarm use case," *IEEE Commun. Mag.*, vol. 56, no. 12, pp. 90–96, Dec. 2018.

[3] 3GPP. (2017). *3GPP: Study on Enhanced Support for Aerial Vehicles*. [Online]. Available: https://portal.3gpp.org/desktopmodules/Specifications/SpecificationDetails.aspx?specificationId=3231

[4] Q. Zhang, M. Jiang, Z. Feng, W. Li, W. Zhang, and M. Pan, "IoT enabled UAV: Network architecture and routing algorithm," *IEEE Internet Things J.*, vol. 6, no. 2, pp. 3727–3742, Apr. 2019.

[5] H. Wu, X. Tao, N. Zhang, and X. Shen, "Cooperative UAV cluster-assisted terrestrial cellular networks for ubiquitous coverage," *IEEE J. Sel. Areas Commun.*, vol. 36, no. 9, pp. 2045–2058, Sep. 2018.

[6] B. Ji, Y. Li, D. Cao, C. Li, S. Mumtaz, and D. Wang, "Secrecy performance analysis of UAV assisted relay transmission for cognitive network with energy harvesting," *IEEE Trans. Veh. Technol.*, vol. 69, no. 7, pp. 7404–7415, Jul. 2020.

[7] E. T. Michailidis, N. Nomikos, P. S. Bithas, D. Vouyioukas, and A. G. Kanatas, "Optimal 3-D aerial relay placement for multi-user MIMO communications," *IEEE Trans. Aerosp. Electron. Syst.*, vol. 55, no. 6, pp. 3218–3229, Dec. 2019.

[8] S. Li, L. Yang, D. B. da Costa, and S. Yu, "Performance analysis of UAV-based mixed RF-UWOC transmission systems," *IEEE Trans. Commun.*, vol. 69, no. 8, pp. 5559–5572, Aug. 2021.

[9] L. Yang, J. Chen, M. O. Hasna, and H.-C. Yang, "Outage performance of UAV-assisted relaying systems with RF energy harvesting," *IEEE Commun. Lett.*, vol. 22, no. 12, pp. 2471–2474, Dec. 2018.

[10] T. Shafique, H. Tabassum, and E. Hossain, "Optimization of wireless relaying with flexible UAV-borne reflecting surfaces," *IEEE Trans. Commun.*, vol. 69, no. 1, pp. 309–325, Jan. 2021.

[11] S. K. Singh, K. Agrawal, K. Singh, C. P. Li, and W. J. Huang, "On UAV selection and position-based throughput maximization in multi-UAV relaying networks," *IEEE Access*, vol. 8, pp. 144039–144050, 2020.

[12] P. S. Bithas, V. Nikolaidis, A. G. Kanatas, and G. K. Karagiannidis, "UAV-to-ground communications: Channel modeling and UAV selection," *IEEE Trans. Commun.*, vol. 68, no. 8, pp. 5135–5144, Aug. 2020.

[13] C. Stefanovic, S. Panic, V. Bhatia, and N. Kumar, "On second-order statistics of the composite channel models for UAV-to-ground communications with UAV selection," *IEEE Open J. Commun. Soc.*, vol. 2, pp. 534–544, 2021.

[14] V. U. Pai and B. Sainath, "UAV selection and link switching policy for hybrid tethered UAV-assisted communication," *IEEE Commun. Lett.*, vol. 25, no. 7, pp. 2410–2414, Jul. 2021.

[15] B. S. Tan, K. H. Li, and K. C. Teh, "Performance analysis of orthogonal space-time block code with minimum-selection generalized selection combining receiver over Rayleigh fading," *IEEE Trans. Veh. Technol.*, vol. 61, no. 3, pp. 1463–1467, Mar. 2012.

[16] X. Yu, W. Xu, S.-H. Leung, and J. Wang, "Unified performance analysis of transmit antenna selection with OSTBC and imperfect CSI over Nakagami-*m* fading channels," *IEEE Trans. Veh. Technol.*, vol. 67, no. 1, pp. 494–508, Jan. 2018.
[17] J. N. Laneman and G. W. Wornell, "Distributed space-time-coded protocols for exploiting cooperative diversity in wireless networks," *IEEE Trans. Inf. Theory*, vol. 49, no. 10, pp. 2415–2425, Oct. 2003.
[18] S.-H. Wu, H.-L. Chiu, and J.-H. Li, "Effectiveness and relay efficiency of opportunistic multipoint relaying on cooperative ARQ," *IEEE Trans. Veh. Technol.*, vol. 66, no. 6, pp. 4781–4796, Jun. 2017.
[19] H.-L. Chiu and S.-H. Wu, "Cross-layer performance analysis of cooperative ARQ with opportunistic multi-point relaying in mobile networks," *IEEE Trans. Wireless Commun.*, vol. 17, no. 6, pp. 4191–4205, Jun. 2018.
[20] H. Zhang, X. Zhang, and D. K. Sung, "An efficient cooperative transmission based opportunistic broadcast scheme in VANETs," *IEEE Trans. Mobile Comput.*, early access, Aug. 19, 2021, doi: 10.1109/TMC.2021.3105982.
[21] H. Murata, A. Kuwabara, and Y. Oishi, "Distributed cooperative relaying based on space-time block code: System description and measurement campaign," *IEEE Access*, vol. 9, pp. 25623–25631, 2021.
[22] I. Ahmad, C. K. Sung, D. Kramarev, G. Lechner, H. Suzuki, and I. Grivell, "Outage probability and ergodic capacity of distributed transmit beamforming with imperfect CSI," *IEEE Trans. Veh. Technol.*, vol. 71, no. 3, pp. 3008–3019, Mar. 2022.
[23] G. Sun, J. Li, Y. Liu, S. Liang, and H. Kang, "Time and energy minimization communications based on collaborative beamforming for UAV networks: A multi-objective optimization method," *IEEE J. Sel. Areas Commun.*, vol. 39, no. 11, pp. 3555–3572, Nov. 2021.
[24] T. Feng, L. Xie, J. Yao, and J. Xu, "UAV-enabled data collection for wireless sensor networks with distributed beamforming," *IEEE Trans. Wireless Commun.*, vol. 21, no. 2, pp. 1347–1361, Feb. 2022.
[25] J. Diao, M. Hedayati, and Y. E. Wang, "Experimental demonstration of distributed beamforming on two flying mini-drones," in *Proc. United States Nat. Committee URSI Nat. Radio Sci. Meeting (USNC-URSI NRSM)*, Jan. 2019, pp. 1–2.
[26] W. Lin, L. Li, J. Yuan, Z. Han, M. Juntti, and T. Matsumoto, "Cooperative lossy communications in unmanned aerial vehicle networks: Age-of-information with outage probability," *IEEE Trans. Veh. Technol.*, vol. 70, no. 10, pp. 10105–10120, Oct. 2021.
[27] D. Zhai, H. Li, X. Tang, R. Zhang, Z. Ding, and F. R. Yu, "Height optimization and resource allocation for NOMA enhanced UAV-aided relay networks," *IEEE Trans. Commun.*, vol. 69, no. 2, pp. 962–975, Feb. 2021.
[28] Q. Wang, X. Li, S. Bhatia, Y. Liu, Linss T. Alex, and S. Bhatia, "UAV-enabled non-orthogonal multiple access networks for ground-air-ground communications," *IEEE Trans. Green Commun. Netw.*, vol. 6, no. 3, pp. 1340–1354, Sep. 2022.
[29] M. K. Simon and M.-S. Alouini, *Digital Communication Over Fading Channels*, 2nd ed. New York, NY, USA: Wiley, 2005.
[30] I. S. Gradshteyn and I. M. Ryzhik, *Table of Integrals, Series, and Products*, 6th ed. New York, NY, USA: Academic, 2000.
[31] A. Al-Hourani, S. Kandeepan, and S. Lardner, "Optimal LAP altitude for maximum coverage," *IEEE Wireless Commun. Lett.*, vol. 3, no. 6, pp. 569–572, Dec. 2014.
[32] P. S. Bithas, A. A. Rontogiannis, and G. K. Karagiannidis, "An improved threshold-based channel selection scheme for wireless communication systems," *IEEE Trans. Wireless Commun.*, vol. 15, no. 2, pp. 1531–1546, Feb. 2016.
[33] P. C. Sofotasios, M. K. Fikadu, S. Muhaidat, Q. Cui, G. K. Karagiannidis, and M. Valkama, "Full-duplex regenerative relaying and energy-efficiency optimization over generalized asymmetric fading channels," *IEEE Trans. Wireless Commun.*, vol. 16, no. 5, pp. 3232–3251, May 2017.
[34] Z. Yao, W. Cheng, W. Zhang, and H. Zhang, "Resource allocation for 5G-UAV-based emergency wireless communications," *IEEE J. Sel. Areas Commun.*, vol. 39, no. 11, pp. 3395–3410, Nov. 2021.
[35] R. I. Bor-Yaliniz, A. El-Keyi, and H. Yanikomeroglu, "Efficient 3-D placement of an aerial base station in next generation cellular networks," in *Proc. IEEE Int. Conf. Commun. (ICC)*, May 2016, pp. 1–5.
[36] V. Aalo and J. Zhang, "Performance analysis of maximal ratio combining in the presence of multiple equal-power cochannel interferers in a Nakagami fading channel," *IEEE Trans. Veh. Technol.*, vol. 50, no. 2, pp. 497–503, Mar. 2001.
[37] A. Bletsas, H. Shin, and M. Z. Win, "Cooperative communications with outage-optimal opportunistic relaying," *IEEE Trans. Wireless Commun.*, vol. 6, no. 9, pp. 3450–3460, Sep. 2007.
[38] P. Maurer, V. Tarokh, and R. Calderbank, "Transmit diversity when the receiver does not know the number of transmit antennas," in *Proc. Int. Symp. Wireless Pers. Multimedia Commun. (WPMC)*, 2001.
[39] B. Sirkeci-Mergen and A. Scaglione, "Randomized space-time coding for distributed cooperative communication," *IEEE Trans. Signal Process.*, vol. 55, no. 10, pp. 5003–5017, Oct. 2007.
[40] Y. Ma and S. Pasupathy, "Efficient performance evaluation for generalized selection combining on generalized fading channels," *IEEE Trans. Wireless Commun.*, vol. 3, no. 1, pp. 29–34, Jan. 2004.
[41] C. M. Bender and S. A. Orszag, *Advanced Mathematical Methods for Scientists and Engineers*. New York, NY, USA: McGraw-Hill, 1978.
[42] A. L. Moustakas and P. Kazakopoulos, "SINR statistics of correlated MIMO linear receivers," *IEEE Trans. Inf. Theory*, vol. 59, no. 10, pp. 6490–6500, Oct. 2013.
[43] H. Ochiai, P. Mitran, H. V. Poor, and V. Tarokh, "Collaborative beamforming for distributed wireless ad hoc sensor networks," *IEEE Trans. Signal Process.*, vol. 53, no. 11, pp. 4110–4124, Nov. 2005.
[44] D. R. Brown, III, and H. V. Poor, "Time-slotted round-trip carrier synchronization for distributed beamforming," *IEEE Trans. Signal Process.*, vol. 56, no. 11, pp. 5630–5643, Nov. 2008.
[45] B. Peiffer, R. Mudumbai, A. Kruger, A. Kumar, and S. Dasgupta, "Experimental demonstration of a distributed antenna array pre-synchronized for retrodirective transmission," in *Proc. Annu. Conf. Inf. Sci. Syst. (CISS)*, Mar. 2016, pp. 460–465.
[46] G. K. Karagiannidis, "A closed-form solution for the distribution of the sum of Nakagami-*m* random phase vectors," *IEEE Commun. Lett.*, vol. 10, no. 12, pp. 828–830, Dec. 2006.
[47] A. A. Khuwaja, Y. Chen, N. Zhao, M.-S. Alouini, and P. Dobbins, "A survey of channel modeling for UAV communications," *IEEE Commun. Surveys Tuts.*, vol. 20, no. 4, pp. 2804–2821, 4th Quart., 2018.
[48] R. Mudumbai, G. Barriac, and U. Madhow, "On the feasibility of distributed beamforming in wireless networks," *IEEE Trans. Wireless Commun.*, vol. 6, no. 5, pp. 1754–1763, May 2007.
[49] I. Dagres, A. Polydoros, and A. Moustakas, "Performance analysis of distributed beamforming in wireless networks: The effect of synchronization and Doppler spread," in *Proc. IEEE Mil. Commun. Conf. (MILCOM)*, Nov. 2021, pp. 957–962.
[50] M. Abramowitz and I. A. Stegun, *Handbook of Mathematical Functions: With Formulas, Graphs, and Mathematical Tables*, vol. 55. North Chelmsford, MA, USA: Courier Corporation, 1964.
[51] A. Prudnikov, Y. Brychkov, and O. Marichev, *Integrals and Series*, vol. 5. London, U.K.: Gordon and Breach Science, 1986.
[52] (2022). *The Wolfram Functions Site*. [Online]. Available: http://functions.wolfram.com

Petros S. Bithas (Senior Member, IEEE) received the Diploma degree in electrical and computer engineering and the Ph.D. degree from the University of Patras, Greece, in 2003 and 2009, respectively. From 2010 to 2020, he was an Associate Researcher at the Department of Digital Systems, University of Piraeus, Greece, where he had been involved in various National and European Research and Development projects. He is currently an Assistant Professor with the Department of Digital Industry Technologies, National and Kapodistrian University of Athens, Greece. His research interests include stochastic modeling and analysis of wireless communications systems. He serves on the Editorial Board of the *International Journal of Electronics and Communications* (Elsevier) and *Telecom* (MDPI).

Aris L. Moustakas (Senior Member, IEEE) received the B.S. degree in physics from Caltech and the M.S. and Ph.D. degrees in theoretical condensed matter physics from Harvard University.

He joined Bell Labs, Lucent Technologies, NJ, USA, in 1998, first at the Physical Sciences Division and then at the Wireless Advanced Technology Laboratory. He is currently an Associate Professor with the Physics Department, National and Kapodistrian University of Athens, Greece. His main research interests include multiple antenna systems, applications of game theory, and statistical physics to communications, networks, and machine learning.

Dr. Moustakas held the DIGITEO Senior Chair in Orsay, France, from 2013 to 2014. He was an Associate Editor of the IEEE TRANSACTIONS ON INFORMATION THEORY from 2009 to 2012.